Supporting information for

Highly C2/C1-Selective Covalent Organic Frameworks Substituted with Azo Groups

Shaofeng Huang[†], Yiming Hu[†], Lili Tan[§], Shun Wan[*, ‡], Sadegh Yazdi[≠], Yinghua Jin[*, ‡], Wei Zhang[*, †]

[†]Department of Chemistry, University of Colorado, Boulder, Colorado 80309, United States

[§]State Key Laboratory of Solidification Processing, Center for Nano Energy Materials, School of Materials Science and Engineering, Northwestern Polytechnical University and Shaanxi Joint Laboratory of Graphene (NPU), Xi'an 710072, China

[‡]NCO Technologies, Longmont, Colorado 80501, United States

[≠]Renewable and Sustainable Energy Institute, University of Colorado Boulder, Boulder, Colorado, 80309, United States

[*]To whom correspondence: wan@ncotechs.com; jinalice@yahoo.com; wei.zhang@colorado.edu

Table of Contents

1. Materials and general methods

All commercially available reagents and solvents were used as received without further purification, unless noted otherwise. Compound **1-H**[1], **2**[2], and triethylene glycol monomethyl ether tosylate[3] were synthesized following previously reported procedures without modification.

Flash column chromatography was performed by using a 100-150 times weight excess of flash silica gel 32-63 μm from Dynamic Absorbants Inc. Fractions were analyzed by TLC using TLC silica gel F254 250 μm precoated-plates from Dynamic Absorbants Inc.

NMR spectra were taken on Bruker 300 and Inova 500 spectrometers. $CHCl_3$ (7.26 ppm) was used as an internal reference in ^1H NMR, and $CHCl_3$ (77.16 ppm) for ^{13}C NMR. NMR data is reported in the following order: chemical shift, multiplicity (s, singlet; d, doublet; t, triplet; q, quartet; m, multiplet), coupling constants (*J*, Hz), number of protons. Solid-state cross polarization magic angle spinning (CP/MAS) NMR spectra were recorded on an Inova 400 NMR spectrometer. Powder X-Ray Diffraction (PXRD) was obtained from Inel CPS 120 diffraction system, using monochromated Cu Kα (λ=1.542 Å) radiation. Elemental analysis (CHN) was performed at University of Illinois at Urbana Champaign. Microanalysis laboratory using Exeter analytical model CE440 CHN analyser.

The FT-IR spectra of starting materials and as-synthesized COFs were obtained from Agilent Technologies Cary 630 FT-IR. Thermogravimetric analyses (TGA) were performed on a thermogravimetric/differential thermal analyzer by heating the samples at 10 °C min^{-1} to 800 °C under nitrogen atmosphere.

The Quantachrome Autosorb ASiQ automated gas sorption analyzer was used to measure N_2 adsorption isotherm. The samples were heated at 120 °C and kept at this temperature for 24 h

under vacuum for activation. Ultra high purity grade (99.999% purity) N_2, CO_2, CH_4, C_2H_2, C_2H_4, C_2H_6 and He, oil-free valves and gas regulators were used for all free space corrections and measurements. For the gas adsorption measurement, the temperatures were controlled by using a refrigerated bath of liquid N_2 (77 K), ice water (273K) and water (295K). The pore size distribution is calculated with Quenched Solid Density Functional Theory (QSDFT) and cylindrical pore model based on the nitrogen sorption isotherms at 77 K using Quantachrome AsiQwin program.

Transmission Electron Microscopy images were obtained on a FEI Tecnai T12, 120 kV TEM.

2. Experimental procedures

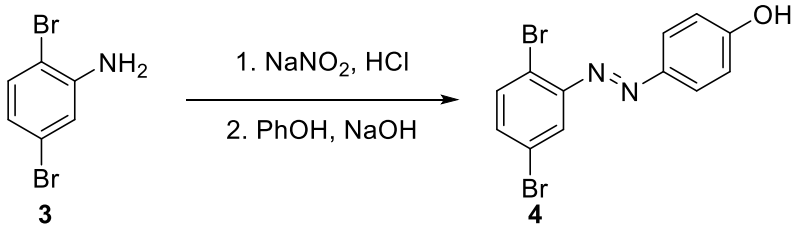

Synthesis of compound 4: The starting material **3** (2.51 g, 10.0 mmol) was dissolved in HCl (1 M, 20 mL, 20 mmol, 2.0 eq.), and the solution was cooled to 0 °C. The aqueous solution of $NaNO_2$ (690 mg, 10.0 mmol, 1.0 eq.) in water (10 mL) was added dropwise. The suspension was stirred at 0 °C for 1 h. To the resulting yellow solution was added a solution of phenol (940 mg, 10.0 mmol) in an aqueous NaOH solution (400 mg, 10.0 mmol, in 5 mL water, 1.0 eq.) dropwise. The mixture turned to dark red and turbid. The suspension was stirred at 0 °C for 2 h and at room temperature for 24 h. The suspension was filtered and the solid was washed with water (100 mL) and dried *in vacuo*. The crude product was purified by flash column chromatography (EtOAc/hexane = 1:20 v:v). The pure compound **4** was obtained as a dark red solid (2.40 g, 70%): ^{1}H NMR (300 MHz, Chloroform-*d*) δ 7.94 (d, *J* = 9.0 Hz, 2H), 7.80 (d, *J* = 2.4 Hz, 1H), 7.59 (d, *J*

= 8.5 Hz, 1H), 7.39 (dd, *J* = 8.5, 2.4 Hz, 1H), 6.96 (d, *J* = 9.0 Hz, 2H), 5.17 (s, 1H). ^{13}C NMR (75 MHz, $CDCl_3$) δ 159.29, 150.36, 147.26, 134.90, 133.92, 126.10, 124.03, 122.12, 121.15, 116.14.

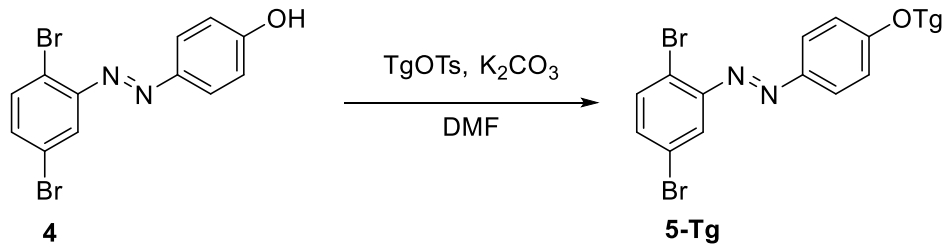

Synthesis of compound 5-Tg: A suspension of the compound **4** (1.03 g, 3.0 mmol), triethylene glycol monomethyl ether tosylate (954 mg, 3.0 mmol, 1.0 eq.) and K_2CO_3 (414 mg, 3.0 mmol, 1.0 eq.) in DMF (15 mL) was heated at 80 °C for 16 h. Water (100 mL) was added and the product was extracted with EtOAc until the aqueous phase turned to colorless. The organic extracts were combined and all the volatiles were removed under reduced pressure. The crude product was purified by flash column chromatography (EtOAc/hexane = 1:2 v:v). The pure compound **5-Tg** was obtained as a dark red oil (1.25 g, 93%): ^{1}H NMR (300 MHz, Chloroform-*d*) δ 7.95 (d, *J* = 9.0 Hz, 2H), 7.79 (d, *J* = 2.4 Hz, 1H), 7.58 (d, *J* = 8.5 Hz, 1H), 7.38 (dd, *J* = 8.5, 2.4 Hz, 1H), 7.03 (d, *J* = 9.0 Hz, 2H), 4.26 – 4.19 (m, 2H), 3.94 – 3.87 (m, 2H), 3.78 – 3.73 (m, 2H), 3.72 – 3.64 (m, 4H), 3.58 – 3.53 (m, 2H), 3.38 (s, 3H). ^{13}C NMR (75 MHz, $CDCl_3$) δ 162.36, 150.36, 147.08, 134.85, 133.81, 125.78, 124.01, 122.08, 121.09, 115.12, 72.06, 71.04, 70.81, 70.73, 69.70, 67.94, 59.18.

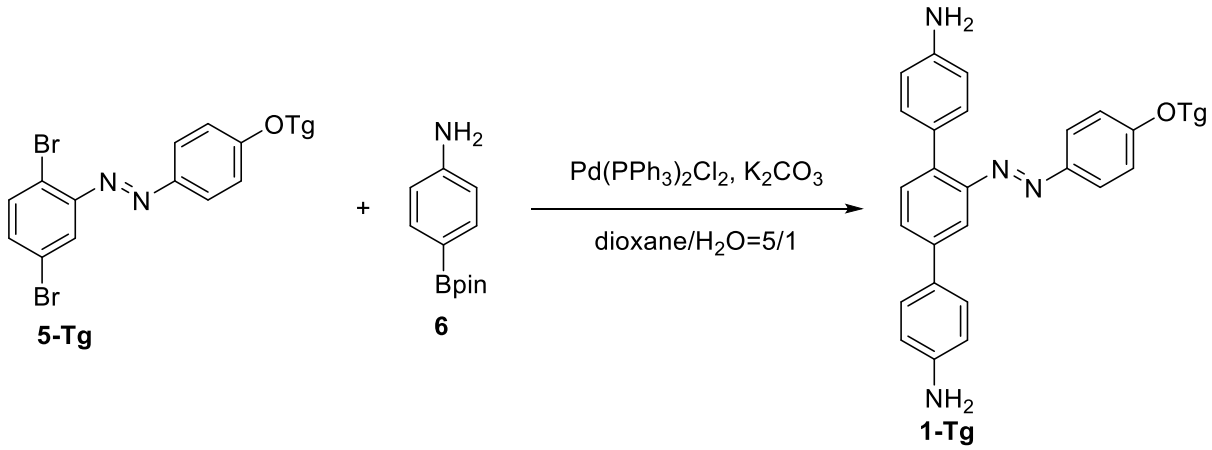

Synthesis of compound 1-Tg: A typical Suzuki coupling procedure was used for the synthesis of compound **1-Tg**. A flame-dried 100 mL Schlenk tube was charged with **5-Tg** (1.34 g, 2.75 mmol), **6** (1.58 g, 7.2 mmol, 2.6 eq.), $Pd(PPh_3)_2Cl_2$ (70 mg, 0.1 mmol, 0.04 eq.) and K_2CO_3 (1.24 g, 9.0 mmol, 3.3 eq.). A mixture of dioxane (45 mL) and H_2O (9 mL) was bubbled with N_2 for 20 min and added to the Schlenk tube. The suspension was heated at 110 °C for 16 h under nitrogen. Water (50 mL) was added and the product was extracted with EtOAc until the aqueous phase turned to colorless. The organic extracts were combined and all the volatiles were removed under reduced pressure. The crude product was purified by flash column chromatography ($MeCN/CH_2Cl_2$=1:4 v:v). The pure product **1-Tg** was obtained as an orange solid (926 mg, 64 %): ^{1}H NMR (500 MHz, Chloroform-*d*) δ 7.85 (d, *J* = 2.0 Hz, 1H), 7.83 (d, *J* = 8.9 Hz, 2H), 7.67 (dd, *J* = 8.0, 2.0 Hz, 1H), 7.57 (d, *J* = 8.1 Hz, 1H), 7.52 (d, *J* = 8.5 Hz, 2H), 7.31 (d, *J* = 8.4 Hz, 2H), 6.99 (d, *J* = 9.0 Hz, 2H), 6.80 – 6.72 (m, 4H), 4.23 – 4.17 (m, 3H), 3.92 – 3.86 (m, 2H), 3.79 – 3.72 (m, 6H), 3.73 – 3.67 (m, 2H), 3.68 – 3.64 (m, 2H), 3.58 – 3.53 (m, 2H), 3.38 (s, 3H). ^{13}C NMR (75 MHz, $CDCl_3$) δ 161.17, 150.01, 147.70, 146.15, 145.78, 140.16, 138.58, 132.10, 130.92, 130.82, 129.14, 128.19, 128.14, 125.18, 72.08, 71.04, 70.82, 70.74, 69.79, 67.85, 59.20.

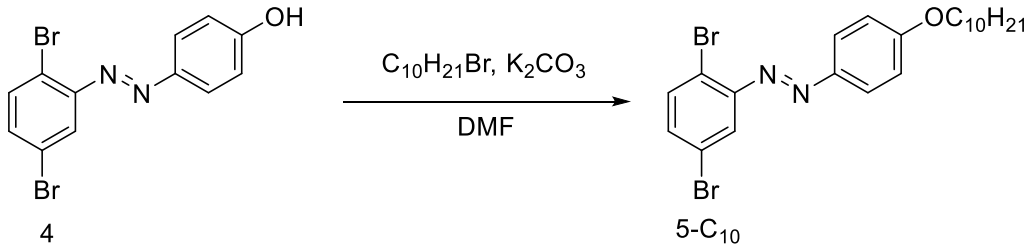

Synthesis of compound 5-C_{10}: A suspension of the compound **4** (684 mg, 2.0 mmol), 1-bromodecane (442 mg, 2.0 mmol, 1.0 eq.) and K_2CO_3 (276 mg, 2.0 mmol, 1.0 eq.) in DMF (10 mL) was heated at 80 °C for 16 h. Water (100 mL) was added and the product was extracted with EtOAc until the aqueous phase turned to colorless. The organic extracts were combined and all the volatiles were removed under a reduced pressure. The crude product was purified by flash column chromatography (pure hexane). The mixture of compound **5-C_{10}** and 1-bromodecane was obtained as a red oil, which was used directly in the following step without further purification.

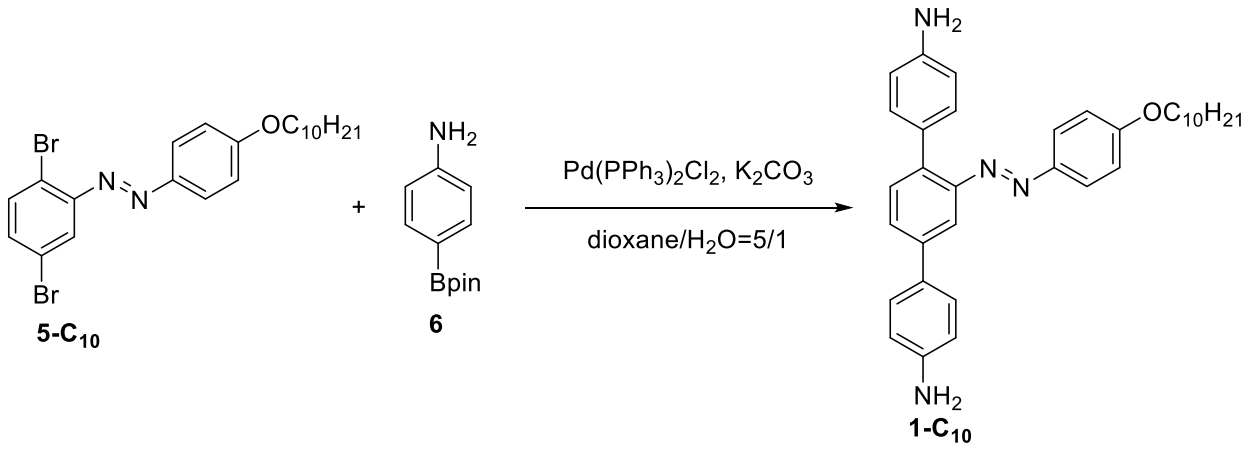

Synthesis of compound 1-C_{10}: A typical Suzuki coupling procedure described above was used for the synthesis of compound **1- C_{10}**. The coupling of the compound **5- C_{10}** (595 mg, 1.34 mmol) and the compound **6** (703 mg, 3.2 mmol, 2.4 eq.) in dioxane (20 mL) and H_2O (4 mL) in the presence of $Pd(PPh_3)_2Cl_2$ (47 mg, 0.07 mmol, 0.05 eq.) and K_2CO_3 (552 mg, 4 mmol, 3 eq.) yielded the product **1- C_{10}** as an orange solid (490 mg, 70 %): ^{1}H NMR (300 MHz, Chloroform-*d*) δ 7.86

(d, *J* = 2.0 Hz, 1H), 7.84 (d, *J* = 8.9 Hz, 2H), 7.67 (dd, *J* = 8.1, 2.0 Hz, 1H), 7.57 (d, *J* = 8.1 Hz, 1H), 7.53 (d, *J* = 8.5 Hz, 2H), 7.32 (d, *J* = 8.5 Hz, 2H), 6.97 (d, *J* = 9.0 Hz, 2H), 6.81 – 6.72 (m, 4H), 4.03 (t, *J* = 6.6 Hz, 2H), 1.90 – 1.73 (m, 2H), 1.30 (m, 14H), 0.98 – 0.76 (m, 3H). ^{13}C NMR (75 MHz, $CDCl_3$) δ 161.60, 150.06, 147.47, 146.13, 145.76, 140.15, 138.49, 132.10, 130.94, 130.79, 129.17, 128.14, 128.10, 125.22, 115.51, 114.80, 114.58, 113.61, 68.48, 32.03, 29.70, 29.52, 29.46, 29.33, 26.15, 25.00, 22.82, 14.26.

3. Solid-State ^{13}C CP-MAS spectra of AzoCOFs

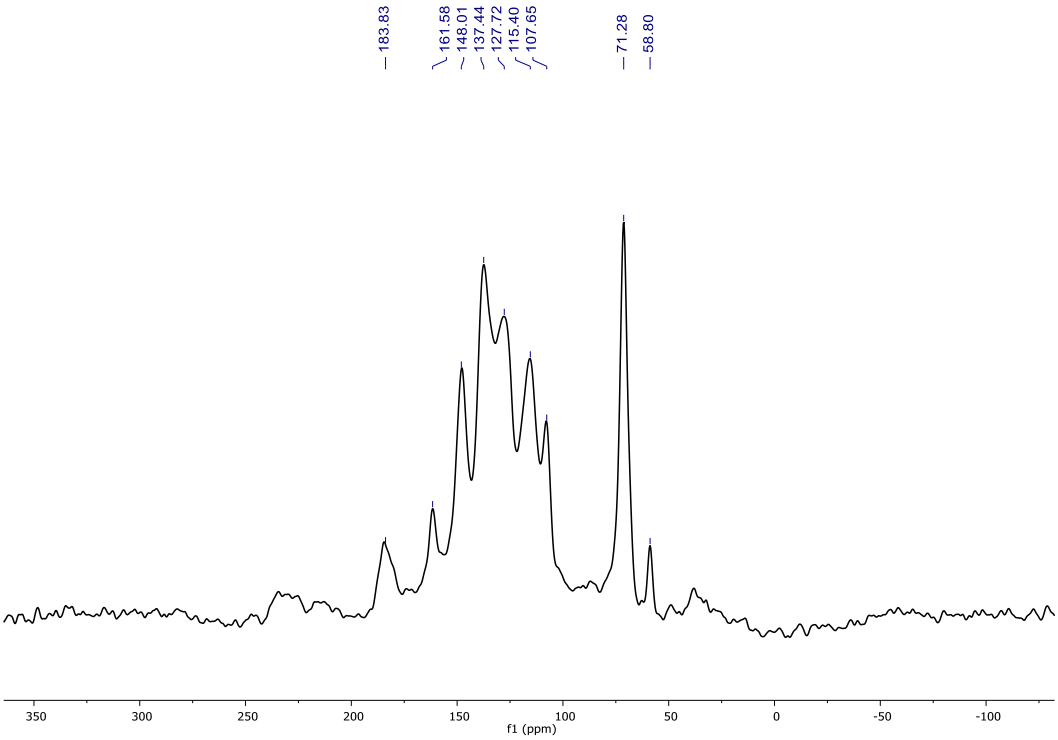

Figure S1. ^{13}C CP/MAS NMR spectrum of **Tg-AzoCOF**.

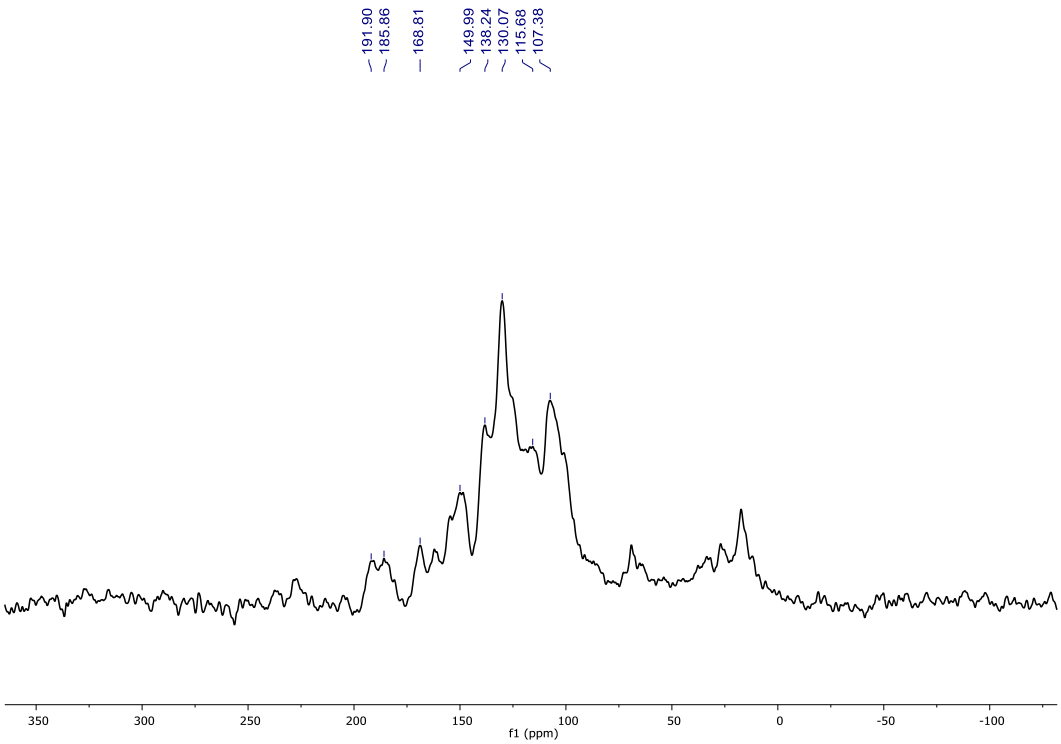

Figure S2. ^{13}C CP/MAS NMR spectrum of **H-AzoCOF**.

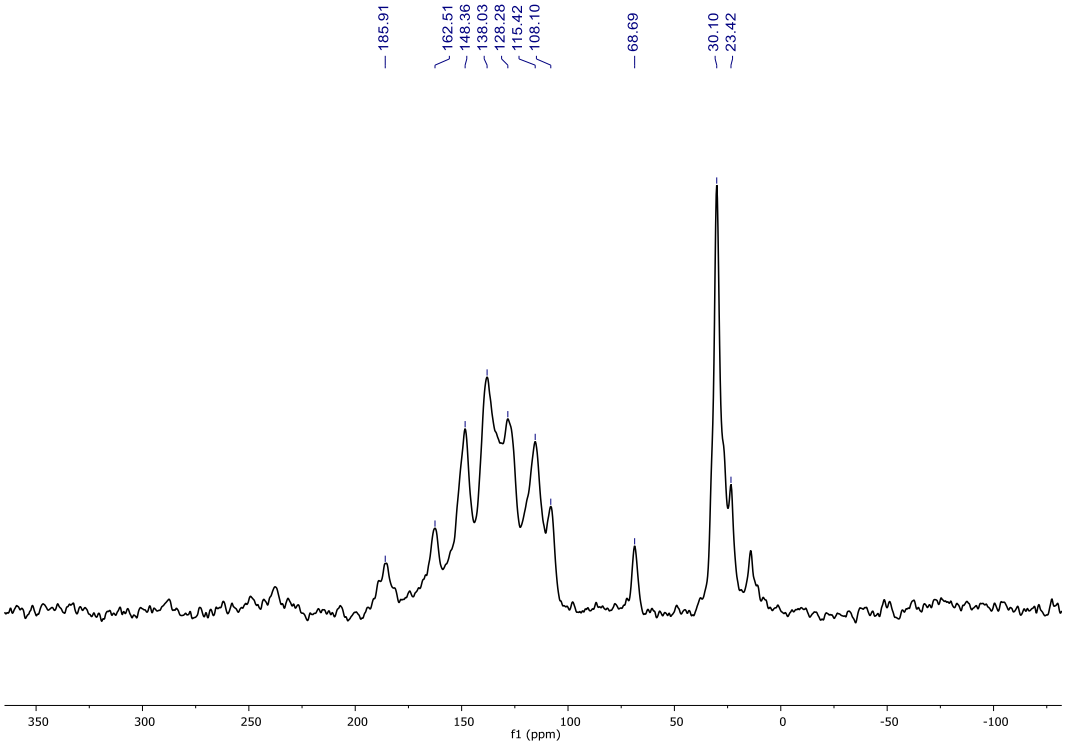

Figure S3. ^{13}C CP/MAS NMR spectrum of **C_{10}-AzoCOF**.

4. FT-IR of AzoCOFs

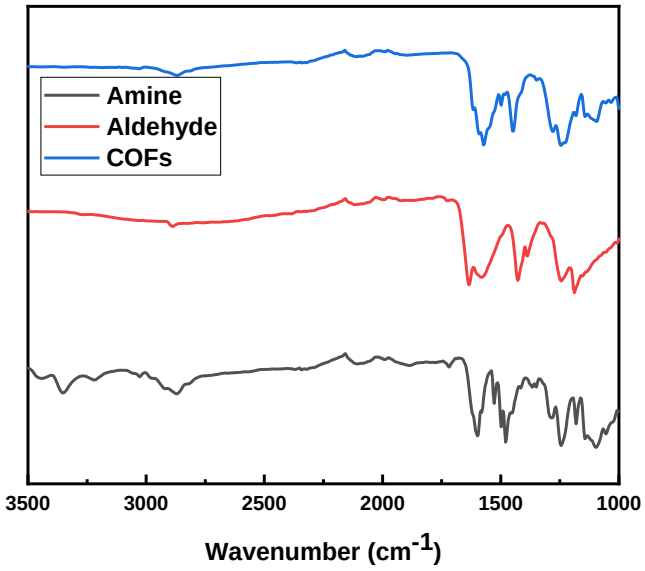

Figure S4. FT-IR spectra of diamine **1-Tg** (black), trialdehyde **2** (red), and **Tg-AzoCOF** (blue).

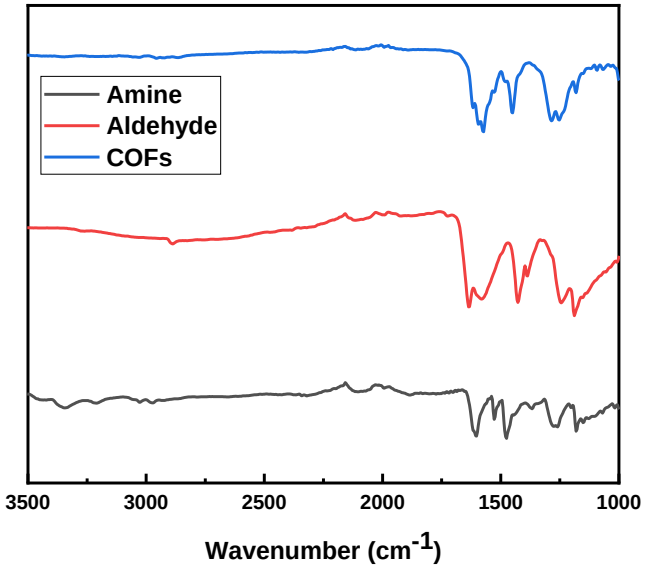

Figure S5. FT-IR spectra of diamine **1-H** (black), trialdehyde **2** (red), and **H-AzoCOF** (blue).

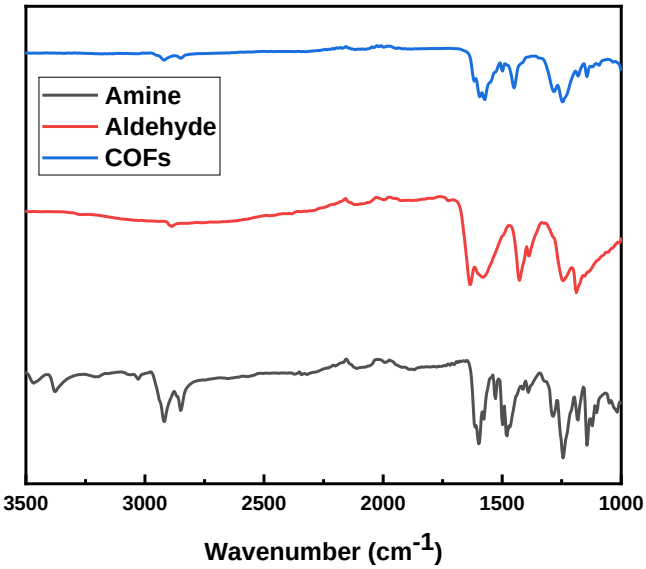

Figure S6. FT-IR spectra of diamine **1-C_{10}** (black), trialdehyde **2** (red), and **C_{10}-AzoCOF** (blue).

5. Powder X-Ray Diffraction of AzoCOFs

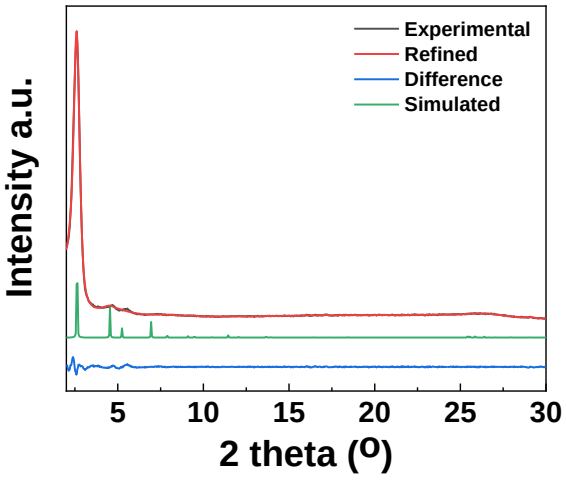

Figure S7. PXRD analysis of **H-AzoCOF**: Observed PXRD patterns (black) refined modeling profile (red), simulated PXRD patterns (green) and difference between the observed PXRD and refined modeling patterns (blue).

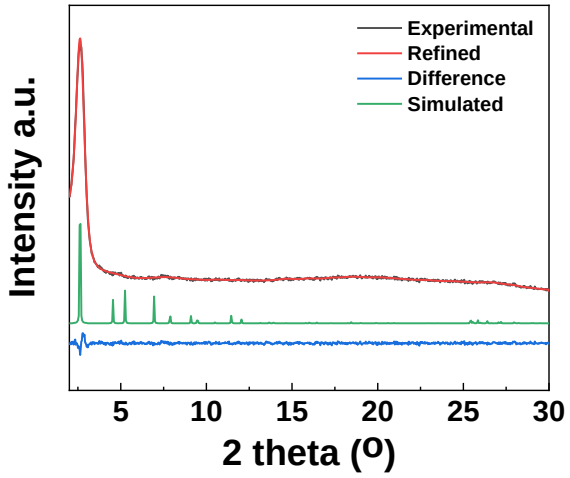

Figure S8. PXRD analysis of **C_{10}-AzoCOF**: Observed PXRD patterns (black) refined modeling profile (red), simulated PXRD patterns (green) and difference between the observed PXRD and refined modeling patterns (blue).

Table S1. Fractional atomic coordinates of **Tg-AzoCOF** unit cell.

Atom	X	Y	Z	Atom	X	Y	Z
N1	1.90437	0.01672	0.3707	C25	1.62518	-0.04507	0.37664
C2	1.88561	0.04212	0.38106	C26	1.63725	-0.07312	0.43594
C3	1.90772	0.08423	0.36667	C27	1.6775	-0.05968	0.51769
C4	1.889	0.10802	0.37433	C28	1.70502	-0.01902	0.53415
C5	1.84709	0.09152	0.39671	C29	1.58683	0.31839	0.35133
C6	1.82517	0.04932	0.41115	C30	1.62481	0.32508	0.32703
C7	1.8438	0.02541	0.40362	C31	1.63352	0.29146	0.31558
C8	1.82749	0.11837	0.40159	O32	1.60679	0.25678	0.29947
C9	1.85154	0.16039	0.37489	C33	2.08676	0.0534	0.34171
C10	1.83543	0.18638	0.37206	C34	2.04556	0.03002	0.31449
C11	1.79402	0.17175	0.39468	C35	2.01496	0.04382	0.29617
C12	1.77021	0.13054	0.42327	O36	2.05481	-0.02491	0.25785
C13	1.78554	0.10418	0.42919	O37	0.27842	0.39203	1.39491
C14	1.77488	0.19802	0.3897	C38	0.24125	0.38309	1.56135
C15	1.79782	0.23982	0.3947	C39	0.20594	0.35115	1.34108
C16	1.77981	0.26382	0.39274	O40	0.1707	0.34642	1.49434
C17	1.73816	0.24741	0.3846	C41	0.14164	0.30844	1.37997
C18	1.71479	0.20563	0.37859	C42	0.10225	0.30725	1.3354
C19	1.73293	0.18153	0.38189	O43	0.07295	0.26904	1.22985

N20	1.72191	0.27433	0.38135	C44	0.03939	0.2724	1.16078
N21	1.75736	0.06258	0.4577	C45	0.00437	0.23181	1.06849
N22	1.72007	0.05009	0.47259	O46	-0.02907	0.2353	0.99709
C23	1.69266	0.00888	0.47276	C47	-0.05875	0.19689	0.90282
C24	1.65261	-0.00436	0.3973				

Table S2. Fractional atomic coordinates of **H-AzoCOF** unit cell.

Atom	X	Y	Z	Atom	X	Y	Z
N1	1.90505	0.0174	-0.03325	C19	1.73277	0.18157	0.00945
C2	1.88619	0.04257	-0.02111	N20	1.7233	0.27539	-0.05576
C3	1.90816	0.08462	-0.04072	N21	1.75821	0.06138	0.07919
C4	1.88932	0.10821	-0.03099	N22	1.72123	0.04882	0.12656
C5	1.84747	0.09143	-0.0007	C23	1.69299	0.0079	0.10818
C6	1.82574	0.04929	0.01891	C24	1.65259	-0.00435	0.14204
C7	1.84448	0.02561	0.0089	C25	1.62403	-0.04475	0.12641
C8	1.82762	0.11788	0.00678	C26	1.6358	-0.07311	0.07744
C9	1.85119	0.15973	-0.03607	C27	1.67613	-0.06108	0.04378
C10	1.83472	0.18534	-0.04102	C28	1.70468	-0.02069	0.05895
C11	1.79343	0.17064	-0.00306	C29	1.5855	0.31648	-0.03545
C12	1.76999	0.12939	0.04332	C30	1.62386	0.32397	-0.02362
C13	1.78581	0.10325	0.05095	C31	1.63361	0.2911	-0.01201
C14	1.77453	0.19723	-0.01617	O32	1.60758	0.25639	0.02259
C15	1.79779	0.23884	-0.05643	C33	2.08578	0.05218	-0.06171
C16	1.78042	0.26342	-0.06964	C34	2.04477	0.02931	-0.08818
C17	1.73898	0.24789	-0.04422	C35	2.01493	0.04386	-0.10581
C18	1.71525	0.20629	-0.00392	O36	2.05311	-0.02604	-0.1436

Table S3. Fractional atomic coordinates of **C_{10}-AzoCOF** unit cell.

Atom	X	Y	Z	Atom	X	Y	Z
N1	1.90382	0.01679	0.37486	C25	1.62303	-0.04391	0.38448
C2	1.88493	0.04206	0.38558	C26	1.63411	-0.07274	0.43833
C3	1.90691	0.08415	0.36986	C27	1.67415	-0.0604	0.51893
C4	1.88806	0.1078	0.37804	C28	1.70246	-0.01995	0.53927
C5	1.84614	0.09112	0.40242	C29	1.58629	0.31839	0.35894
C6	1.82437	0.04894	0.41806	C30	1.62425	0.32502	0.33514
C7	1.84313	0.0252	0.40993	C31	1.63292	0.29138	0.32373
C8	1.82641	0.11779	0.40816	O32	1.60617	0.25673	0.30723
C9	1.85039	0.15978	0.38115	C33	2.08604	0.05329	0.34557

C10	1.83423	0.18571	0.3789	C34	2.04485	0.02995	0.31831
C11	1.79287	0.1711	0.40238	C35	2.01432	0.04382	0.30008
C12	1.76911	0.1299	0.43149	O36	2.05403	-0.02498	0.26193
C13	1.78447	0.10353	0.43696	O37	0.28239	0.39521	1.3898
C14	1.7738	0.19741	0.39743	C38	0.24578	0.38805	1.55564
C15	1.79681	0.2392	0.40127	C39	0.20969	0.35595	1.34604
C16	1.77891	0.26328	0.39899	C40	0.17409	0.36069	1.43073
C17	1.73729	0.24699	0.39167	C41	0.13663	0.32464	1.28819
C18	1.71384	0.20522	0.38688	C42	0.10268	0.3332	1.30141
C19	1.73187	0.18102	0.39048	C43	0.06442	0.29641	1.18582
N20	1.72116	0.274	0.3881	C44	0.03164	0.3066	1.15875
N21	1.75623	0.06191	0.46567	C45	-0.00706	0.26974	1.05488
N22	1.71904	0.04974	0.4838	C46	-0.03924	0.2806	1.01058
C23	1.69102	0.00871	0.48307	C47	-0.07807	0.24377	0.90984
C24	1.65119	-0.0035	0.4092				

6. TGA of AzoCOFs

Samples were run on a TA Instruments Q-500 series thermal gravimetric analyzer with samples held in a platinum pan under nitrogen atmosphere. A 10 K min^{-1} ramp rate was used.

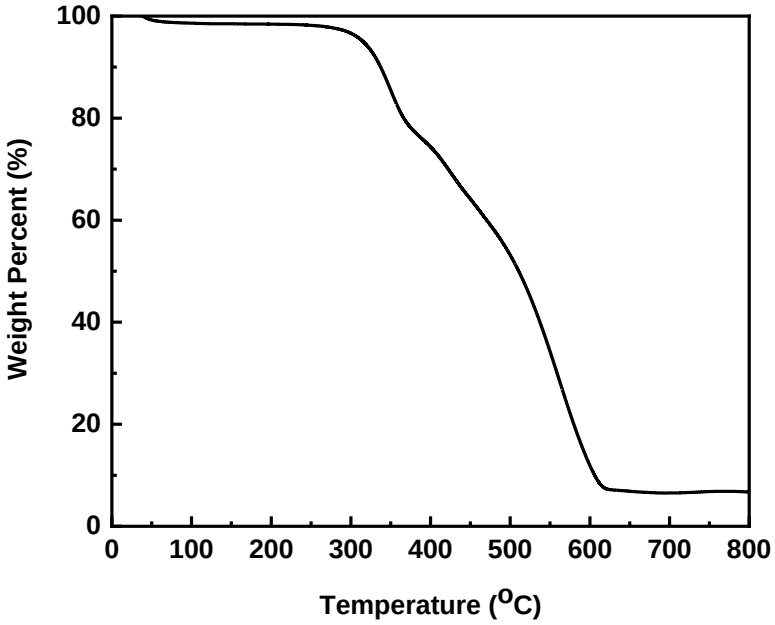

Figure S9. TGA of **Tg-AzoCOF**.

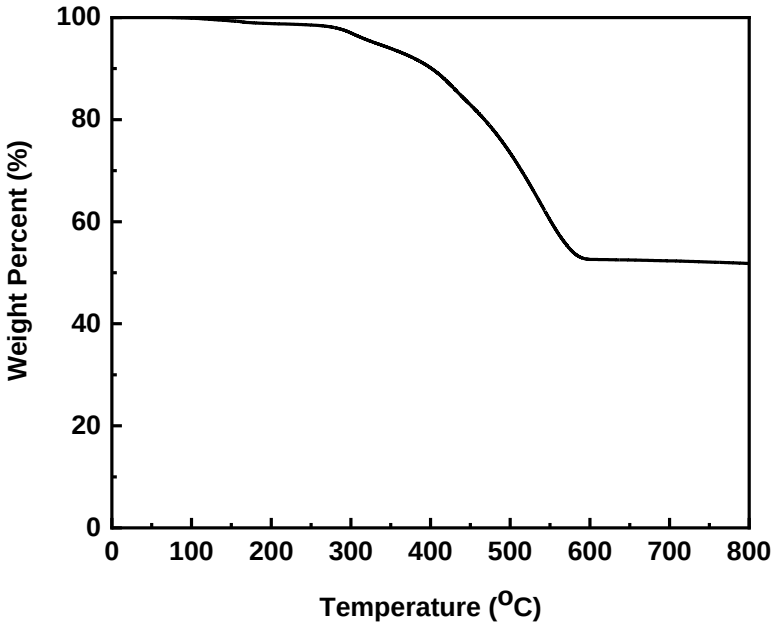

Figure S10. TGA of **H-AzoCOF**.

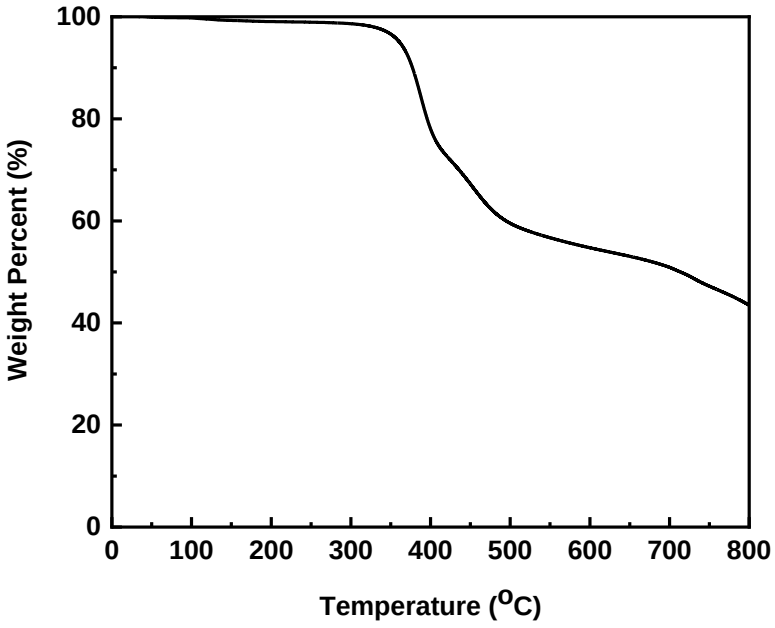

Figure S11. TGA of **C_{10}-AzoCOF**.

7. Additional adsorption data of AzoCOFs

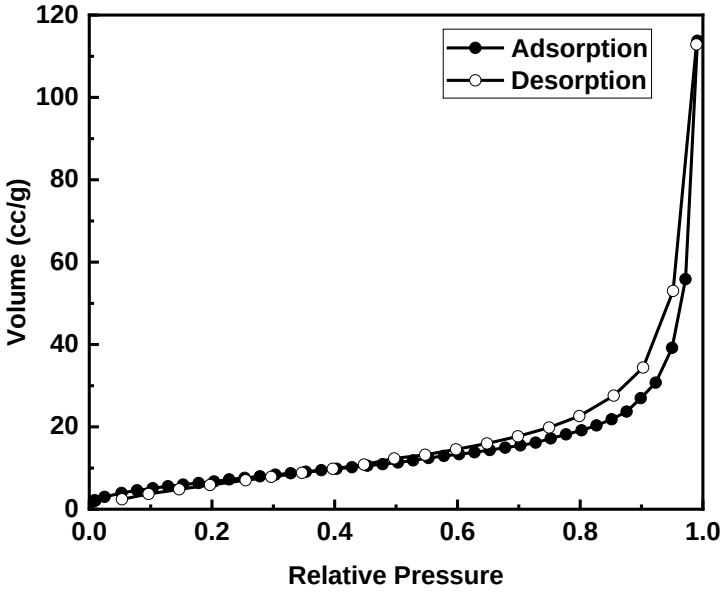

Figure S12. N_2 Adsorption Isotherms of **Tg-AzoCOF** at 77 K.

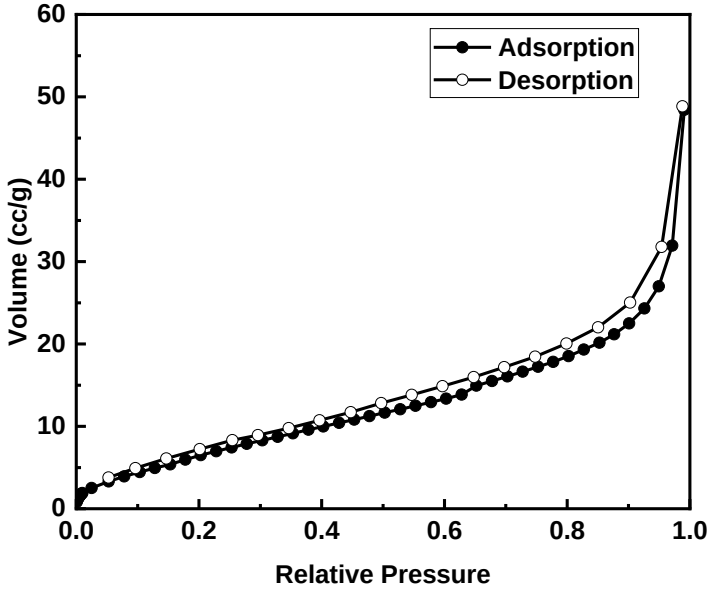

Figure S13. N_2 Adsorption Isotherms of **C_{10}-AzoCOF** at 77 K.

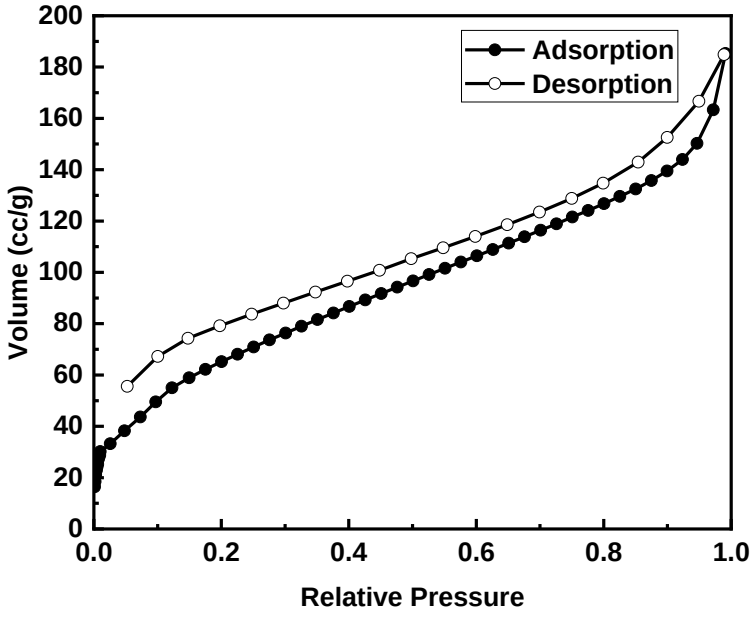

Figure S14. N_2 Adsorption Isotherms of **H-AzoCOF** at 77 K.

Table S4. Surface Area Calculation Based on the BET Model of N_2 Adsorption.

COFs	$S_{BET}/m^2\ g^{-1}$	Pressure Range P/P_0	Points	C Constant	Correlation Coefficient
H-AzoCOF	245	0.05~0.35	11	40.911	0.999158

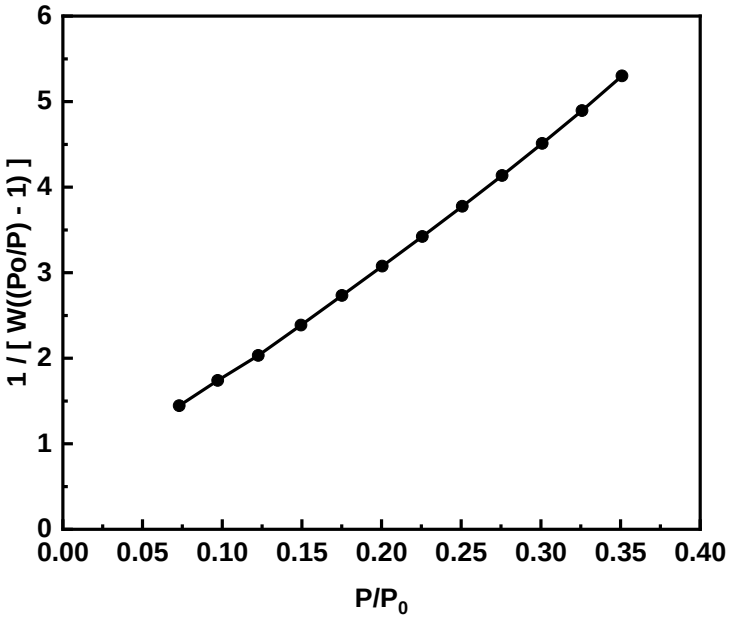

Figure S15. BET Surface Area of **H-AzoCOF** Based on N_2 Adsorption Isotherms.

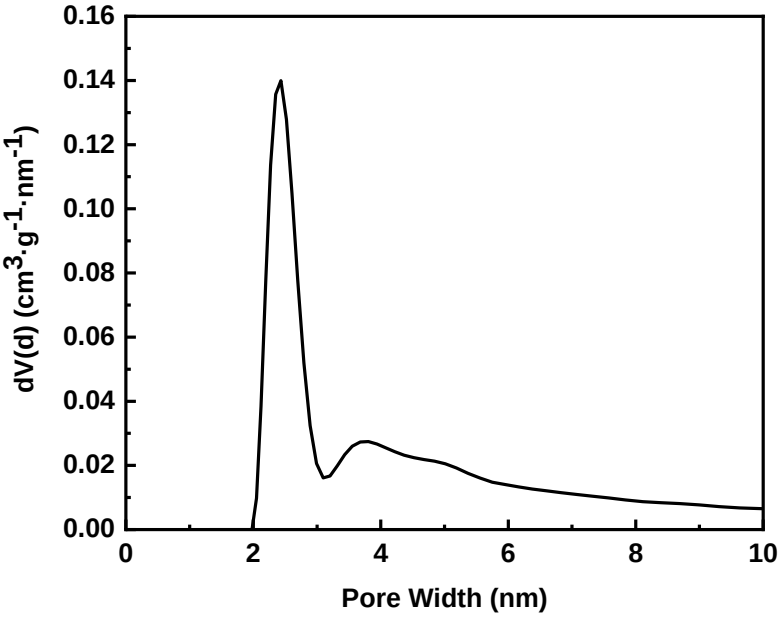

Figure S16. Pore Size Distribution of **H-AzoCOF**.

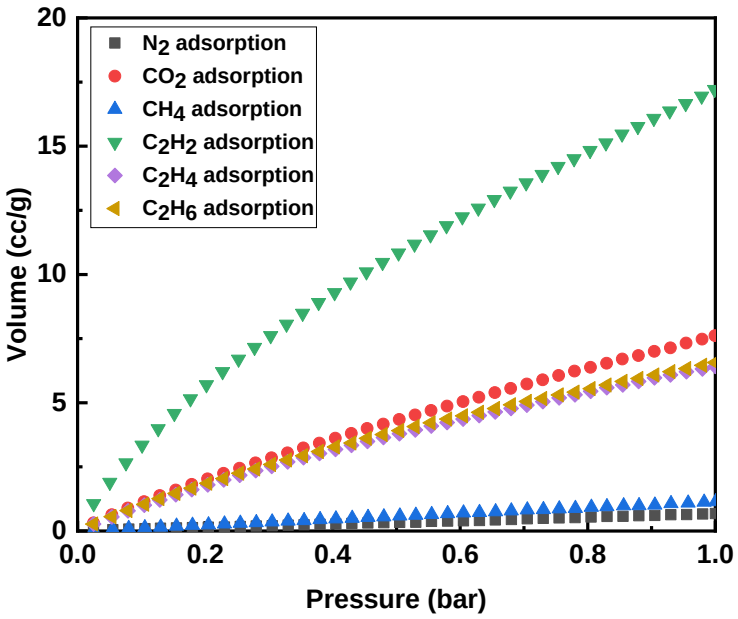

Figure S17. Gas Adsorption Isotherms of **Tg-AzoCOF** at 295 K.

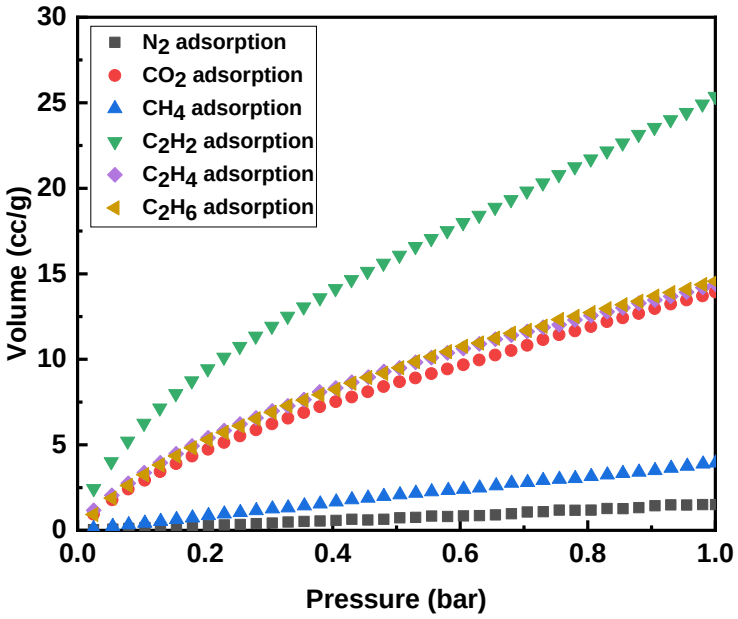

Figure S18. Gas Adsorption Isotherms of **H-AzoCOF** at 295 K.

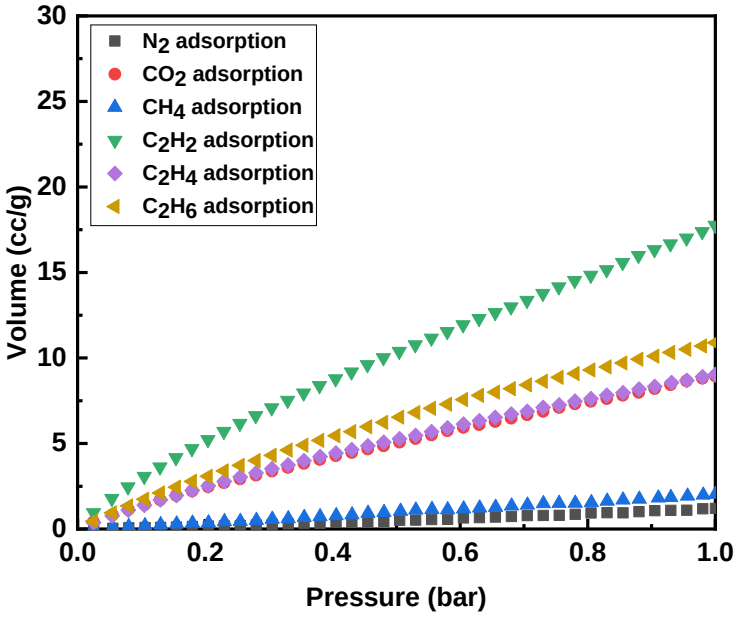

Figure S19. Gas Adsorption Isotherms of **C_{10}-AzoCOF** at 295 K.

8. Additional IAST calculation results of AzoCOFs

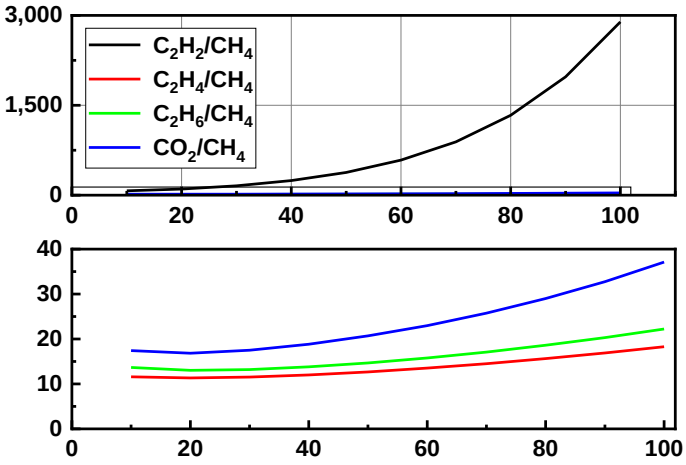

Figure S20. Gas adsorption selectivity with 50:50 ratio gas mixture of **Tg-AzoCOF** at 273 K predicted by IAST.

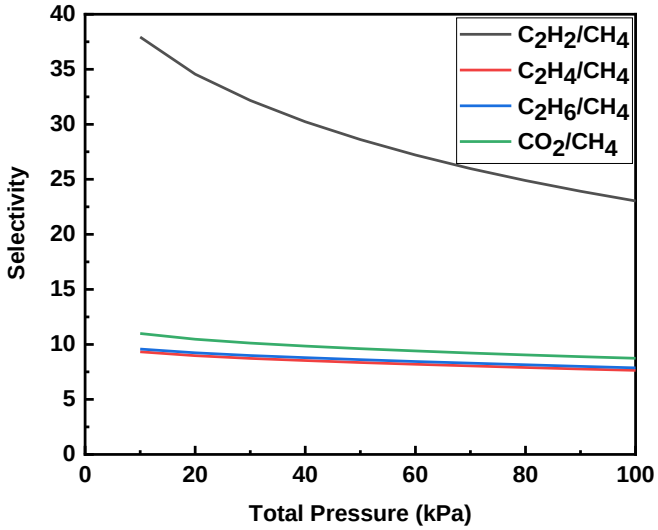

Figure S21. Gas adsorption selectivity with 50:50 ratio gas mixture of **Tg-AzoCOF** at 295 K predicted by IAST.

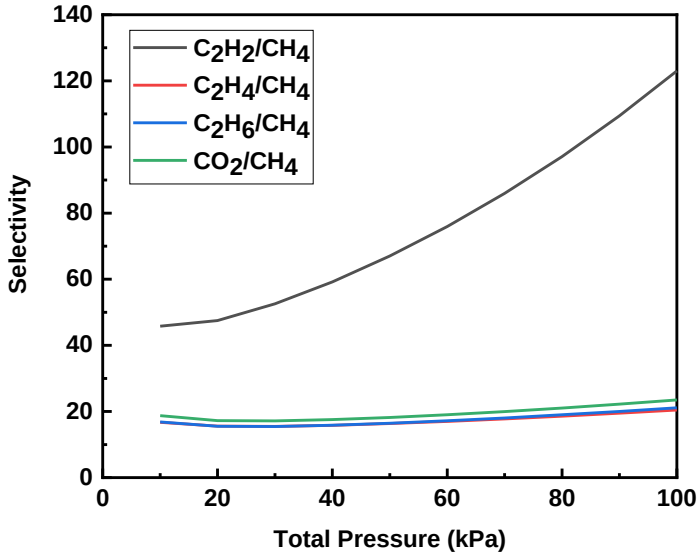

Figure S22. Gas adsorption selectivity with 50:50 ratio gas mixture of **H-AzoCOF** at 273 K predicted by IAST.

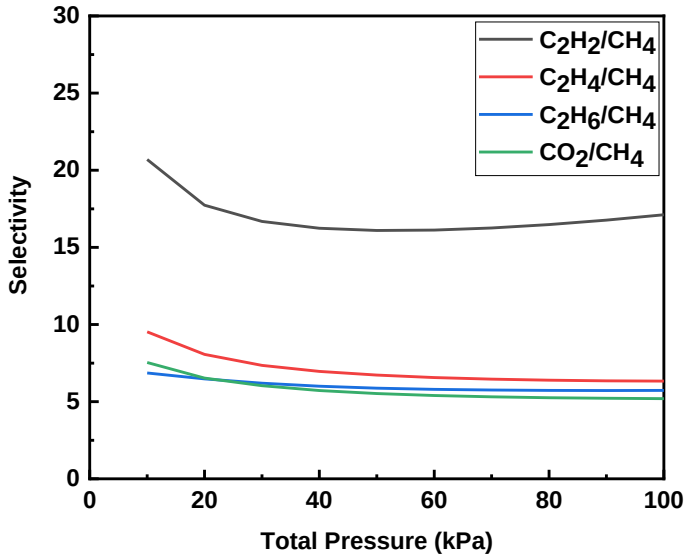

Figure S23. Gas adsorption selectivity with 50:50 ratio gas mixture of **H-AzoCOF** at 295 K predicted by IAST.

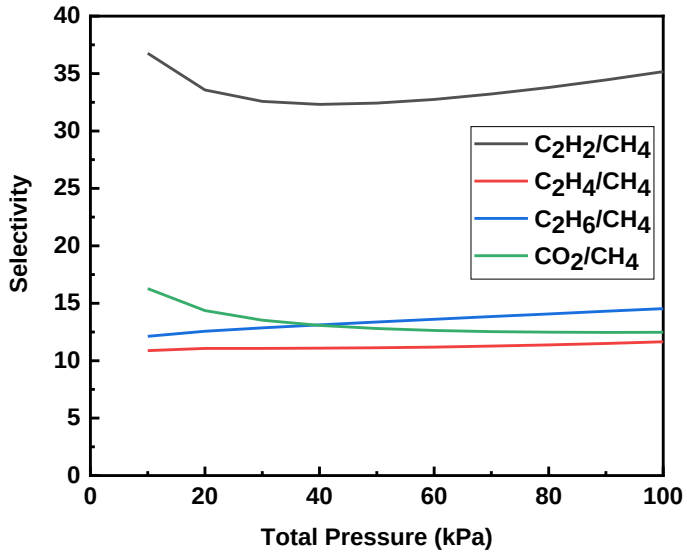

Figure S24. Gas adsorption selectivity with 50:50 ratio gas mixture of **C_{10}-AzoCOF** at 273 K predicted by IAST.

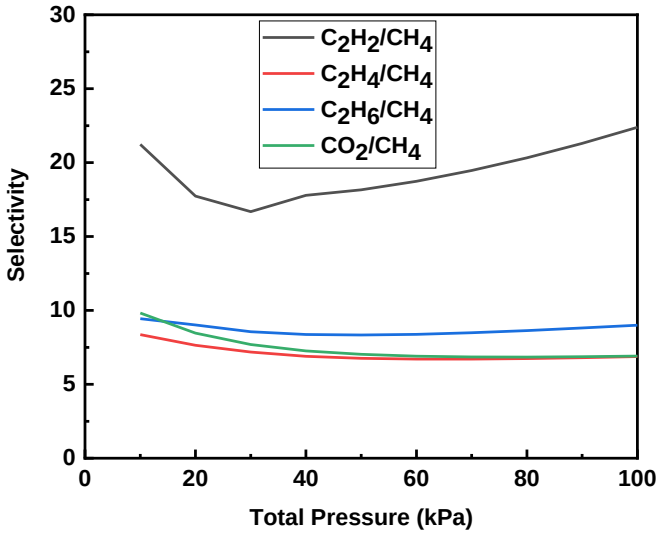

Figure S25. Gas adsorption selectivity with 50:50 ratio gas mixture of **C_{10}-AzoCOF** at 295 K predicted by IAST.

9. Estimation of adsorption heat of AzoCOFs

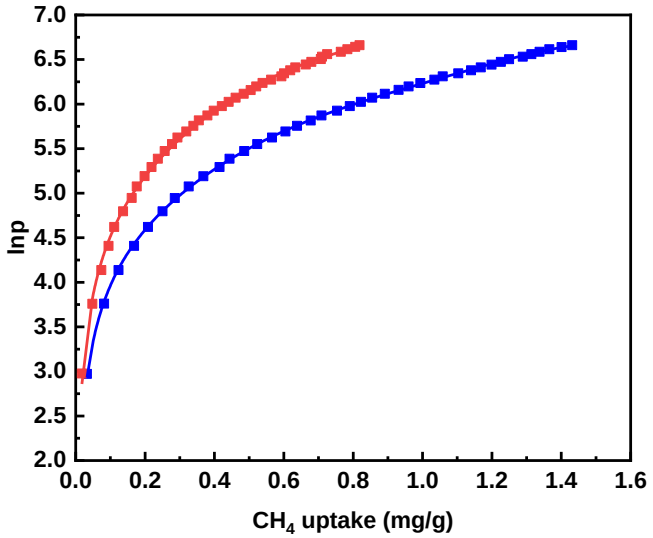

Figure S26. Virial Analysis of CH_4 Adsorption Isotherms of **Tg-AzoCOF** at 273 K (blue) and 295 K (red).

Table S5. Virial Equation Fitting Results of CH_4 Adsorption of **Tg-AzoCOF**.

a_0	a_1	a_2	a_3	a_4	a_5	b_0	b_1	b_2	R^2
-1785.85	-2692.5	3735.34	-2562.37	1682.47	-412.504	12.95887	7.76923	-7.04061	0.99998

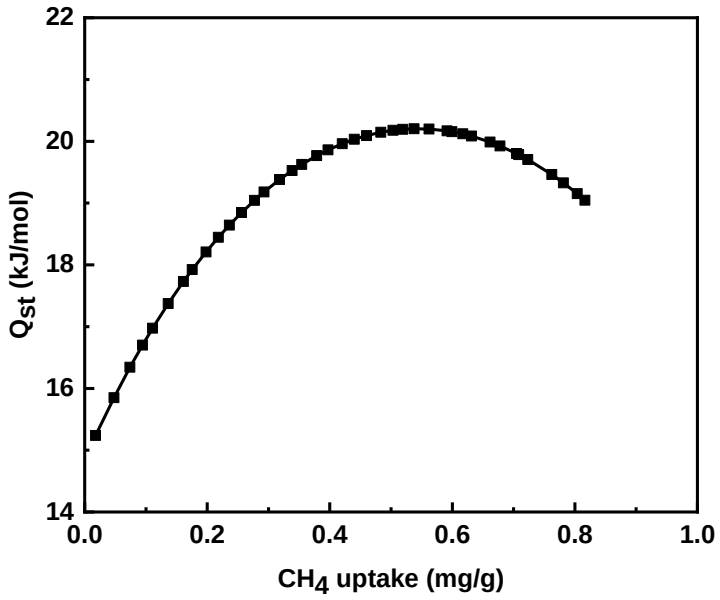

Figure S27. Isosteric Heat of CH_4 Adsorption of **Tg-AzoCOF**.

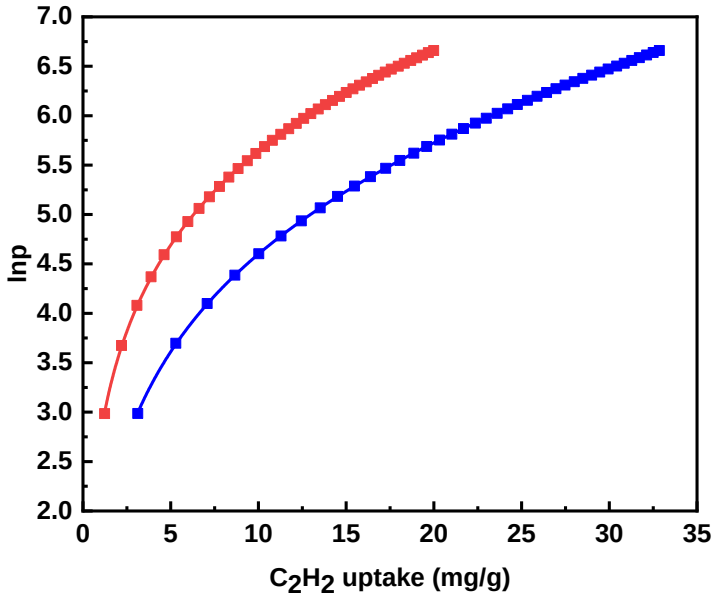

Figure S28. Virial Analysis of C_2H_2 Adsorption Isotherms of **Tg-AzoCOF** at 273 K (blue) and 295 K (red).

Table S6. Virial Equation Fitting Results of C_2H_2 Adsorption of **Tg-AzoCOF**.

a_0	a_1	a_2	a_3	a_4	a_5	b_0	b_1	b_2	R^2
-4090.4	30.25817	-0.90116	0.08409	-0.00204	1.97E-05	16.52674	0.00728	-0.00338	0.99999

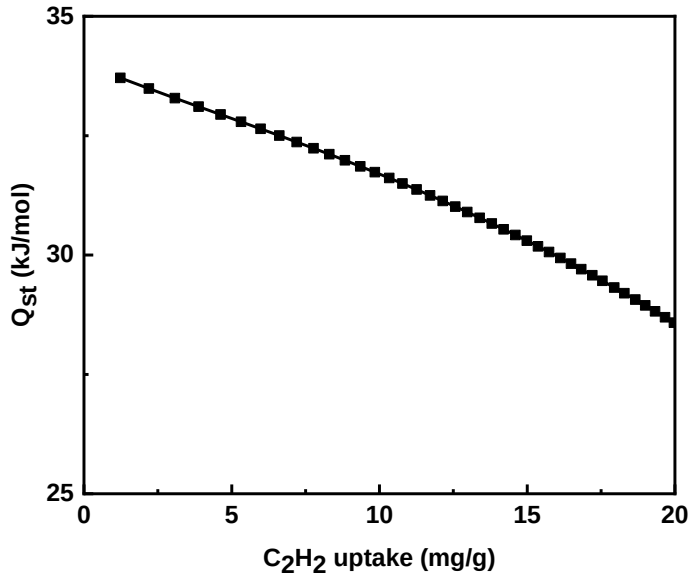

Figure S29. Isosteric Heat of C_2H_2 Adsorption of **Tg-AzoCOF**.

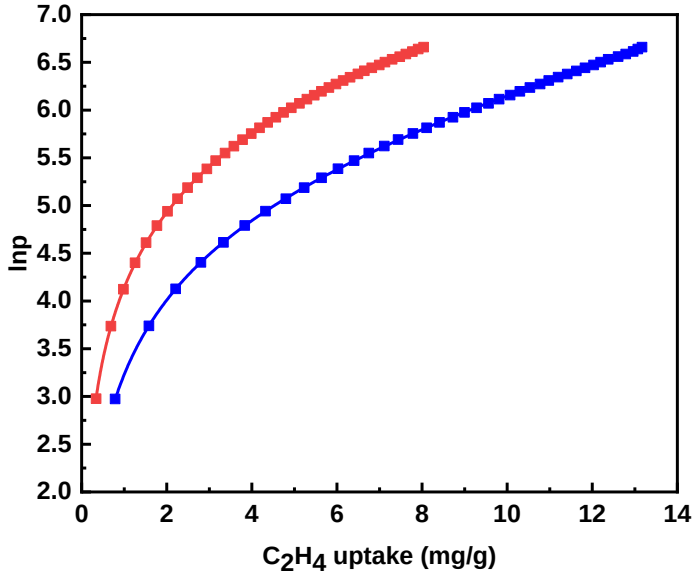

Figure S30. Virial Analysis of C_2H_4 Adsorption Isotherms of **Tg-AzoCOF** at 273 K (blue) and 295 K (red).

Table S7. Virial Equation Fitting Results of C_2H_4 Adsorption of **Tg-AzoCOF**.

a_0	a_1	a_2	a_3	a_4	a_5	b_0	b_1	b_2	R^2
-3295.76	-44.0586	4.18532	0.853	-0.06064	0.00166	15.18816	0.29293	-0.0363	0.99999

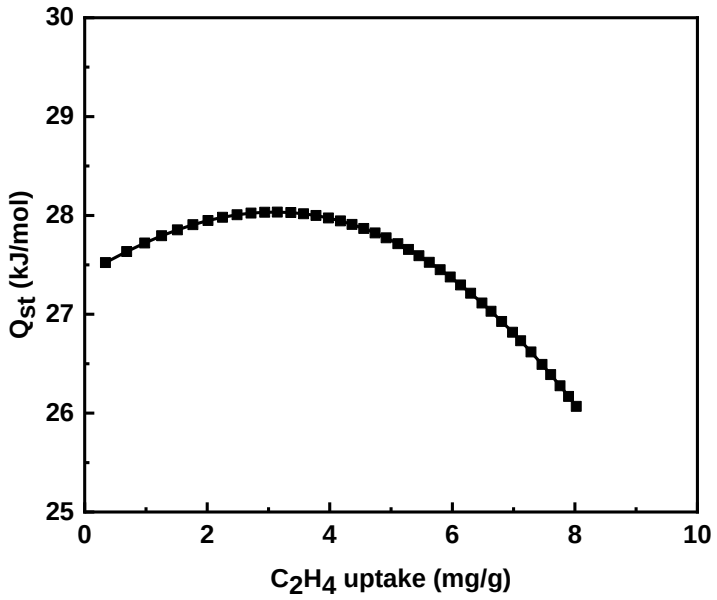

Figure S31. Isosteric Heat of C_2H_4 Adsorption of **Tg-AzoCOF**.

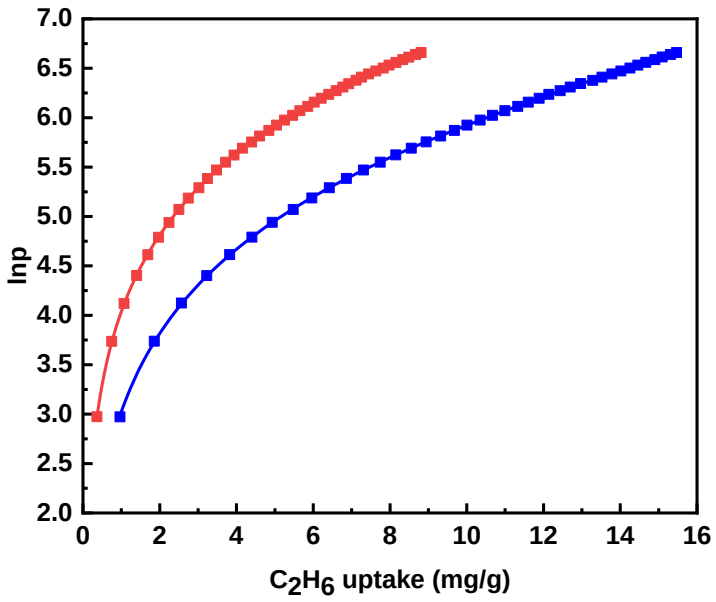

Figure S32. Virial Analysis of C_2H_6 Adsorption Isotherms of **Tg-AzoCOF** at 273 K (blue) and 295 K (red).

Table S8. Virial Equation Fitting Results of C_2H_6 Adsorption of **Tg-AzoCOF**.

a_0	a_1	a_2	a_3	a_4	a_5	b_0	b_1	b_2	R^2
-3781.23	76.4081	-5.1039	0.16264	-0.00378	1.77E-05	16.76064	-0.15573	0.00874	0.99997

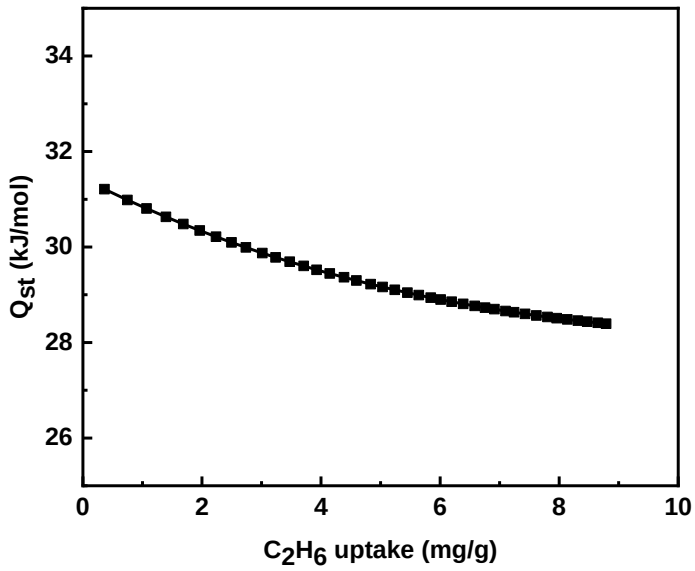

Figure S33. Isosteric Heat of C_2H_6 Adsorption of **Tg-AzoCOF**.

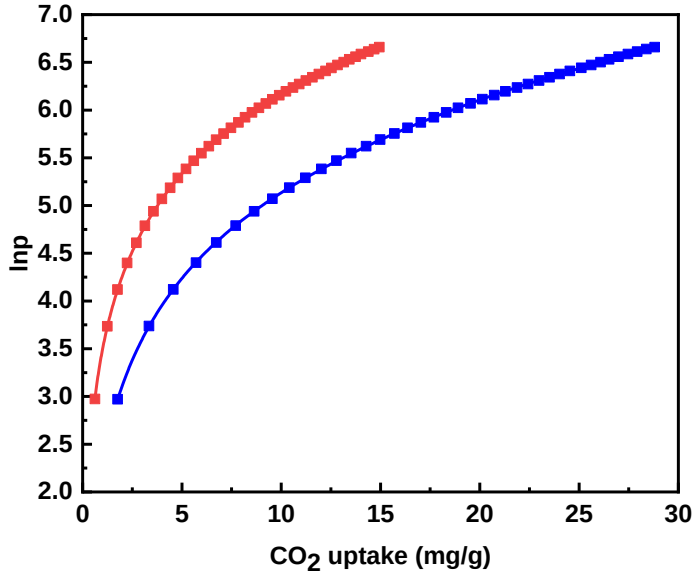

Figure S34. Virial Analysis of CO_2 Adsorption Isotherms of **Tg-AzoCOF** at 273 K (blue) and 295 K (red).

Table S9. Virial Equation Fitting Results of CO_2 Adsorption of **Tg-AzoCOF**.

A_0	a_1	a_2	a_3	a_4	a_5	b_0	b_1	b_2	R^2
-4343.55	78.49639	-3.54269	0.18037	-0.00539	6.28E-05	18.12236	-0.16286	0.00184	0.99998

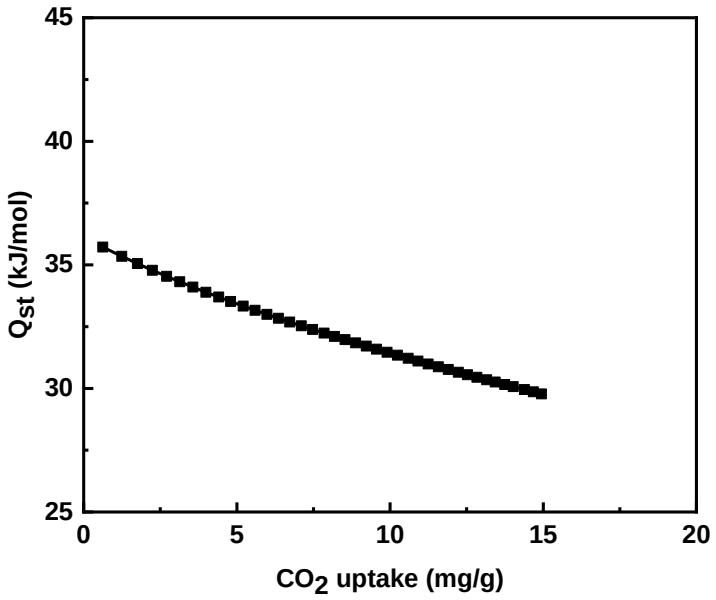

Figure S35. Isosteric Heat of CO_2 Adsorption of **Tg-AzoCOF**.

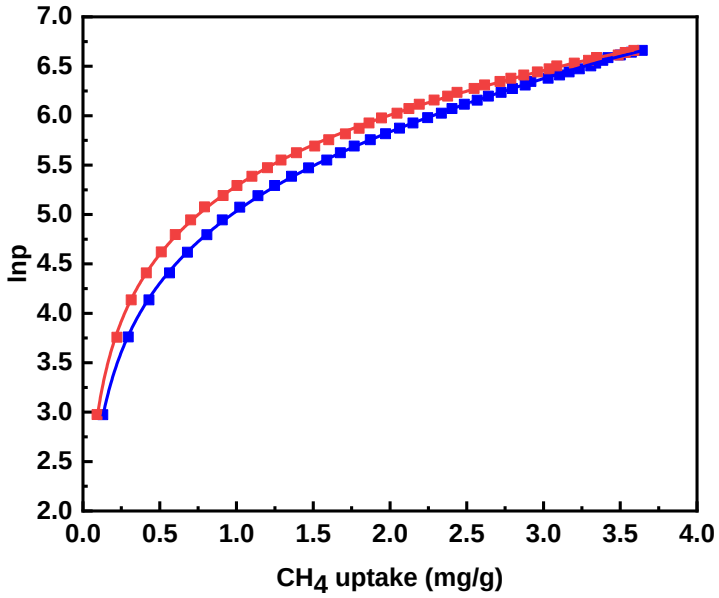

Figure S36. Virial Analysis of CH_4 Adsorption Isotherms of **H-AzoCOF** at 273 K (blue) and 295 K (red).

Table S10. Virial Equation Fitting Results of CH_4 Adsorption of **H-AzoCOF**.

A_0	a_1	a_2	a_3	a_4	a_5	b_0	b_1	b_2	R^2
-1200.17	223.4831	77.06909	-38.113	9.96402	-0.98271	9.41048	-0.9536	-0.02059	0.99979

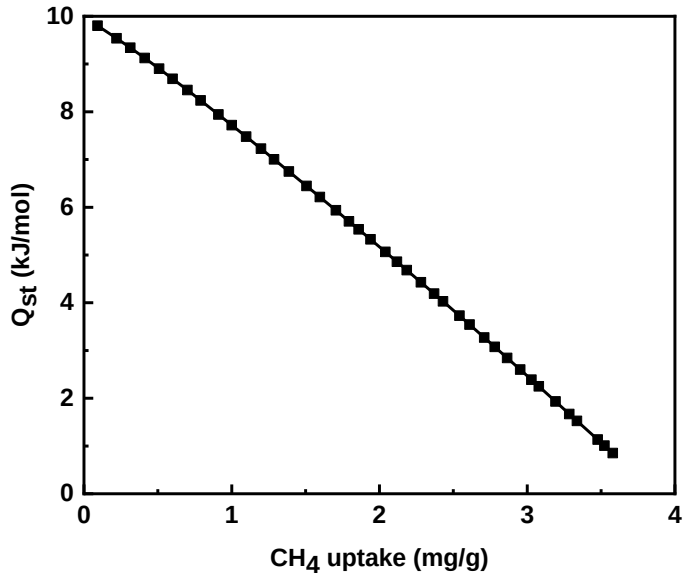

Figure S37. Isosteric Heat of CH_4 Adsorption of **H-AzoCOF**.

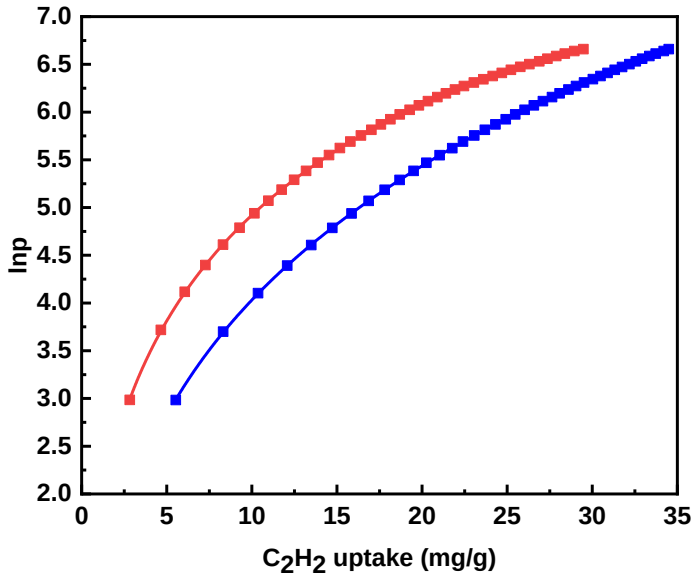

Figure S38. Virial Analysis of C_2H_2 Adsorption Isotherms of **H-AzoCOF** at 273 K (blue) and 295 K (red).

Table S11. Virial Equation Fitting Results of C_2H_2 Adsorption of **H-AzoCOF**.

A_0	a_1	a_2	a_3	a_4	a_5	b_0	b_1	b_2	R^2
-3981.48	75.04342	-1.06492	0.10719	-0.00242	2.18E-05	15.02509	-0.08081	-0.00575	0.99979

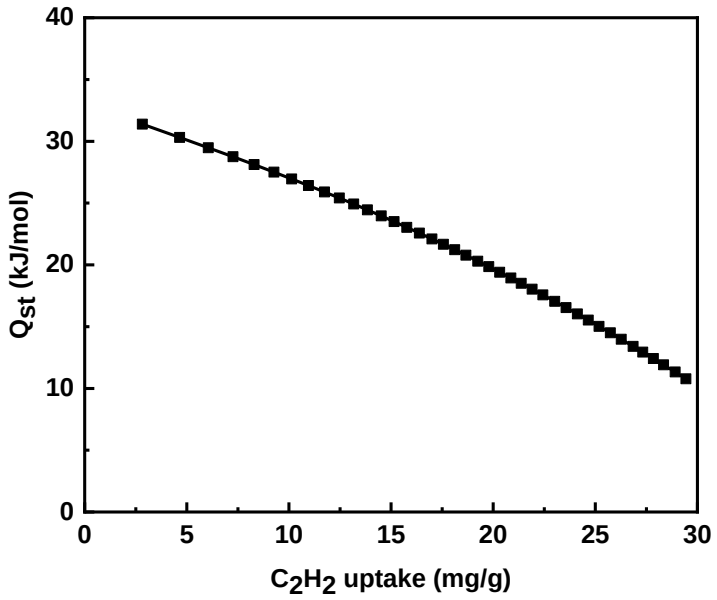

Figure S39. Isosteric Heat of C_2H_2 Adsorption of **H-AzoCOF**.

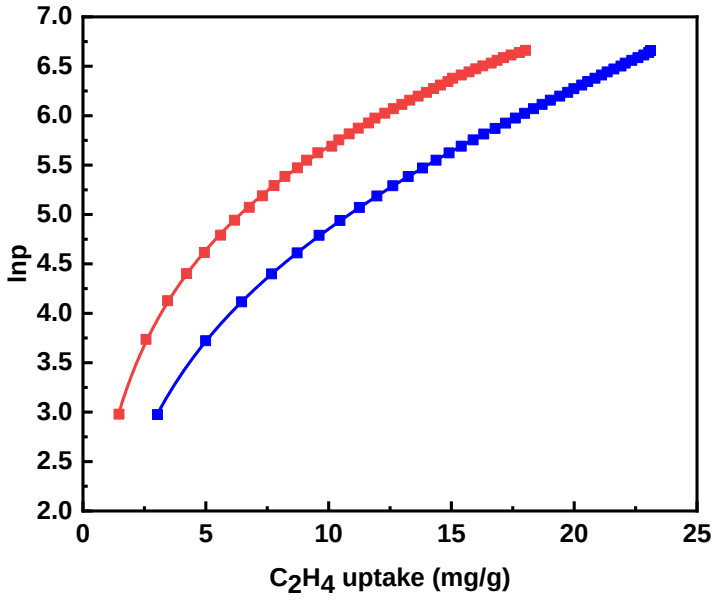

Figure S40. Virial Analysis of C_2H_4 Adsorption Isotherms of **H-AzoCOF** at 273 K (blue) and 295 K (red).

Table S12. Virial Equation Fitting Results of C_2H_4 Adsorption of **H-AzoCOF**.

A_0	a_1	a_2	a_3	a_4	a_5	b_0	b_1	b_2	R^2
-3682.31	70.63471	-3.63363	0.42053	-0.0157	2.32E-04	14.82781	-0.03167	-0.00779	0.99979

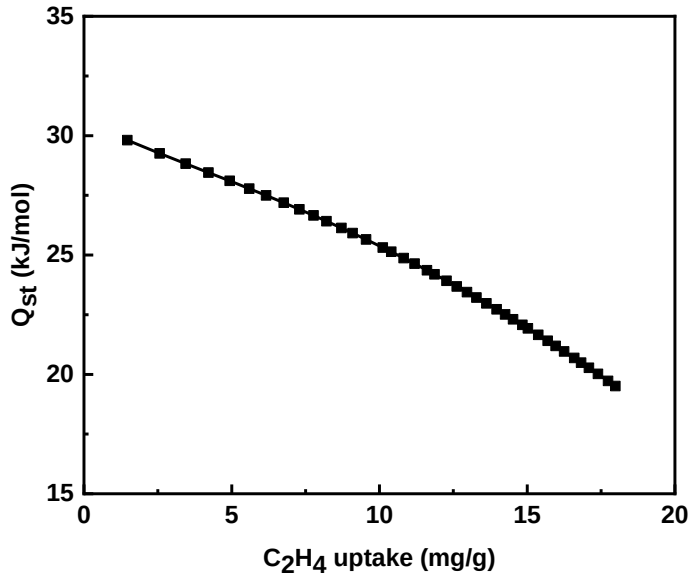

Figure S41. Isosteric Heat of C_2H_4 Adsorption of **H-AzoCOF**.

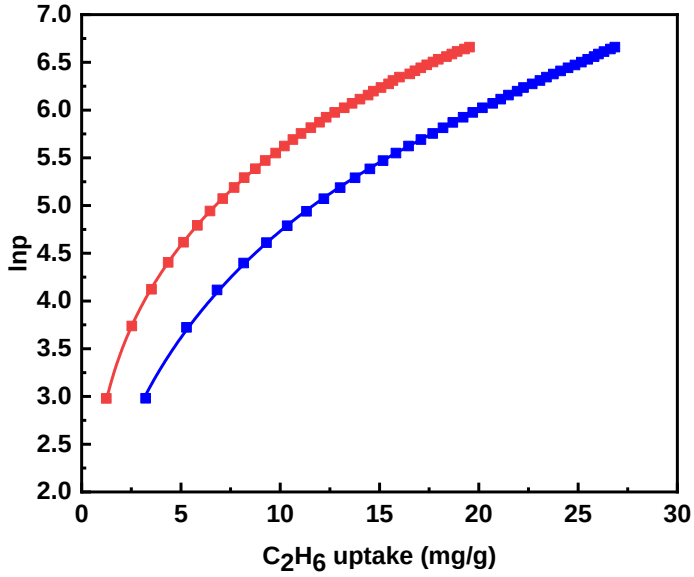

Figure S42. Virial Analysis of C_2H_6 Adsorption Isotherms of **H-AzoCOF** at 273 K (blue) and 295 K (red).

Table S13. Virial Equation Fitting Results of C_2H_6 Adsorption of **H-AzoCOF**.

A_0	a_1	a_2	a_3	a_4	a_5	b_0	b_1	b_2	R^2
-4003.98	90.43744	1.21452	-0.25482	0.00968	-1.28E-04	16.26465	-0.2752	0.00451	0.99979

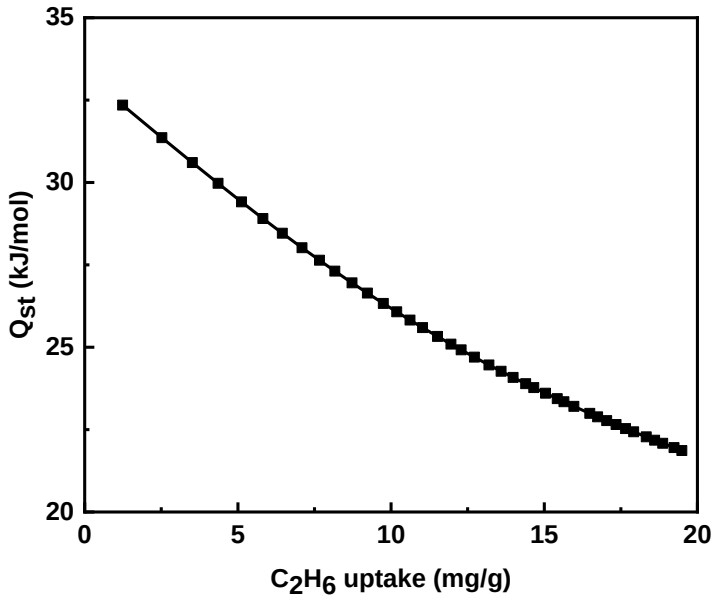

Figure S43. Isosteric Heat of C_2H_6 Adsorption of **H-AzoCOF**.

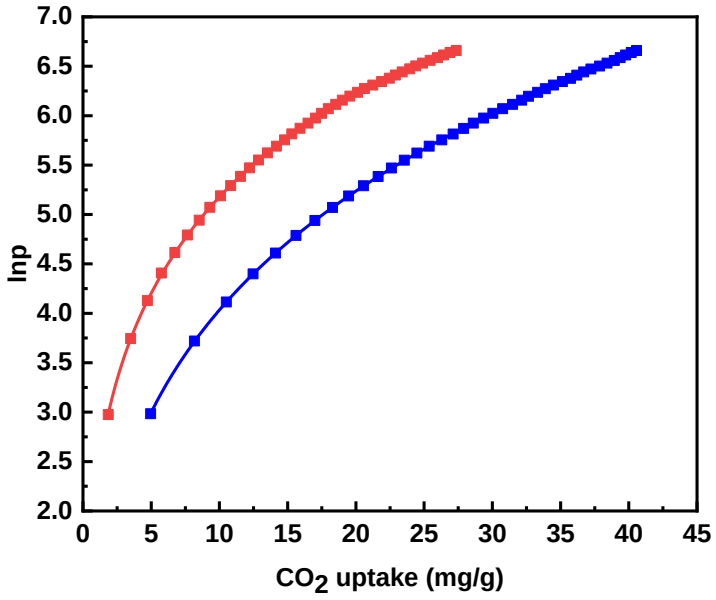

Figure S44. Virial Analysis of CO_2 Adsorption Isotherms of **H-AzoCOF** at 273 K (blue) and 295 K (red).

Table S14. Virial Equation Fitting Results of CO_2 Adsorption of **H-AzoCOF**.

A_0	a_1	a_2	a_3	a_4	a_5	b_0	b_1	b_2	R^2
-4597.15	34.03239	0.50867	0.02131	-3.64E-04	2.82E-06	17.78586	-0.02337	-0.0048	0.99979

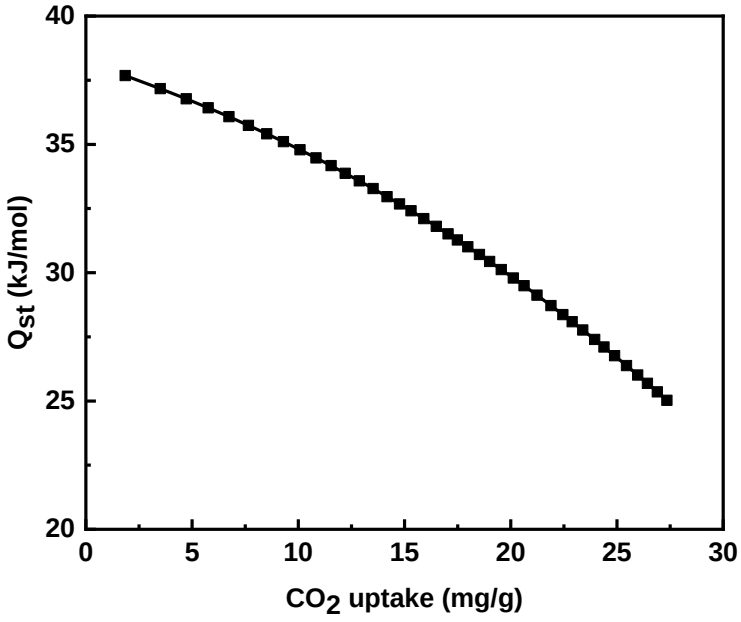

Figure S45. Isosteric Heat of CO_2 Adsorption of **H-AzoCOF**.

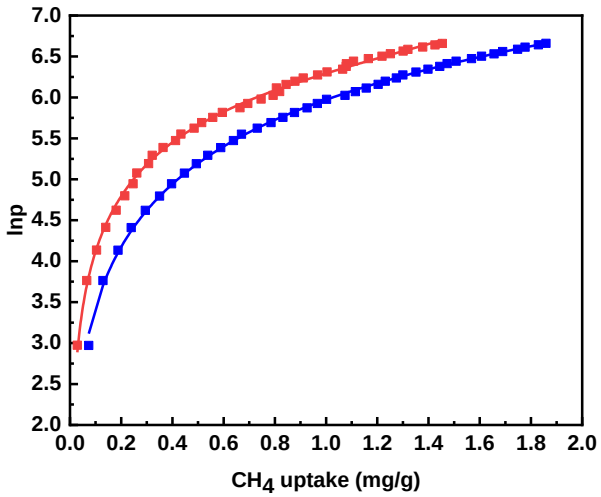

Figure S46. Virial Analysis of CH_4 Adsorption Isotherms of **C_{10}-AzoCOF** at 273 K (blue) and 295 K (red).

Table S15. Virial Equation Fitting Results of CH_4 Adsorption of **C_{10}-AzoCOF**.

a_0	a_1	a_2	a_3	a_4	a_5	b_0	b_1	b_2	R^2
-2750.13	2647.475	-1069.89	-34.928	42.68766	-10.50461	15.76139	-9.16099	3.67685	0.99845

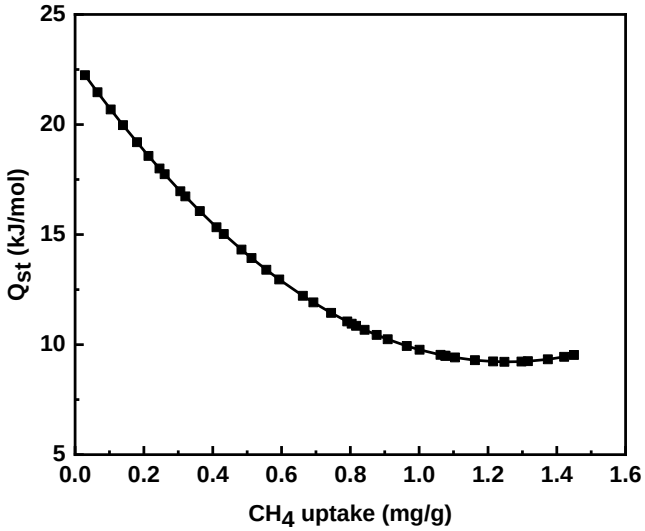

Figure S47. Isosteric Heat of CH_4 Adsorption of **C_{10}-AzoCOF**.

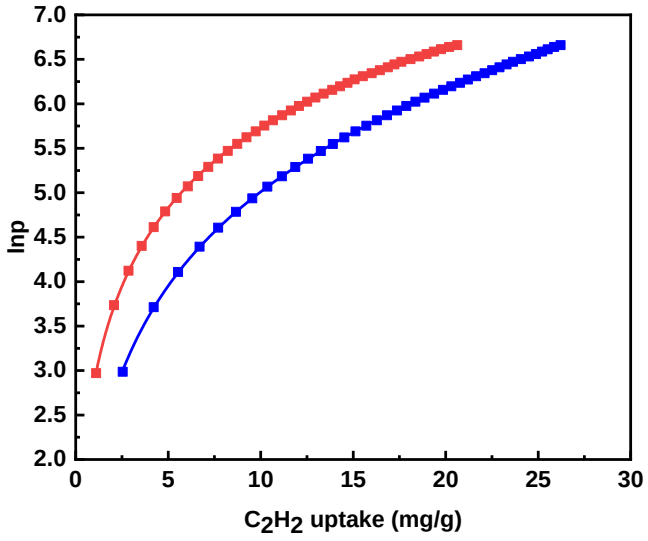

Figure S48. Virial Analysis of C_2H_2 Adsorption Isotherms of **C_{10}-AzoCOF** at 273 K (blue) and 295 K (red).

Table S16. Virial Equation Fitting Results of C_2H_2 Adsorption of **C_{10}-AzoCOF**.

a_0	a_1	a_2	a_3	a_4	a_5	b_0	b_1	b_2	R^2
-3926.04	164.0068	-5.4334	0.27212	-0.00865	0.000109508	16.03335	-0.40062	0.00323	0.99996

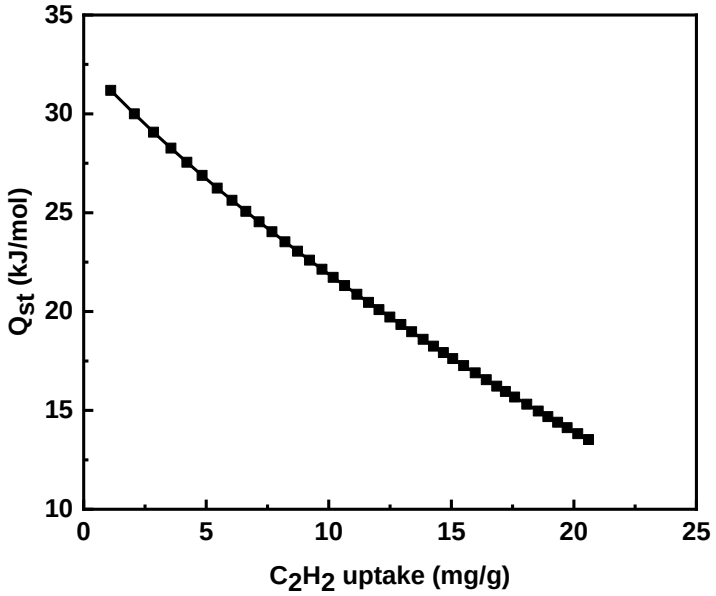

Figure S49. Isosteric Heat of C_2H_2 Adsorption of **C_{10}-AzoCOF**.

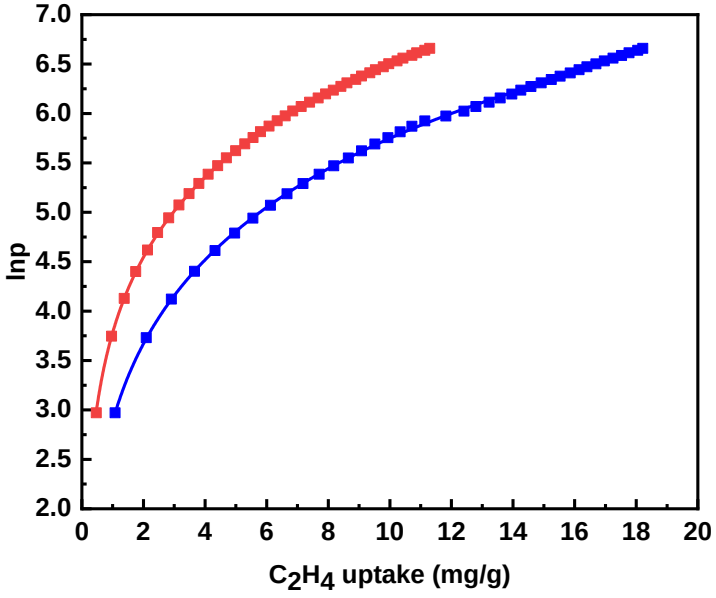

Figure S50. Virial Analysis of C_2H_4 Adsorption Isotherms of **C_{10}-AzoCOF** at 273 K (blue) and 295 K (red).

Table S17. Virial Equation Fitting Results of C_2H_4 Adsorption of **C_{10}-AzoCOF**.

a_0	a_1	a_2	a_3	a_4	a_5	b_0	b_1	b_2	R^2
-3376.79	92.52776	-3.91326	0.15639	-0.00925	0.000243518	15.14954	-0.22724	0.00659	0.99989

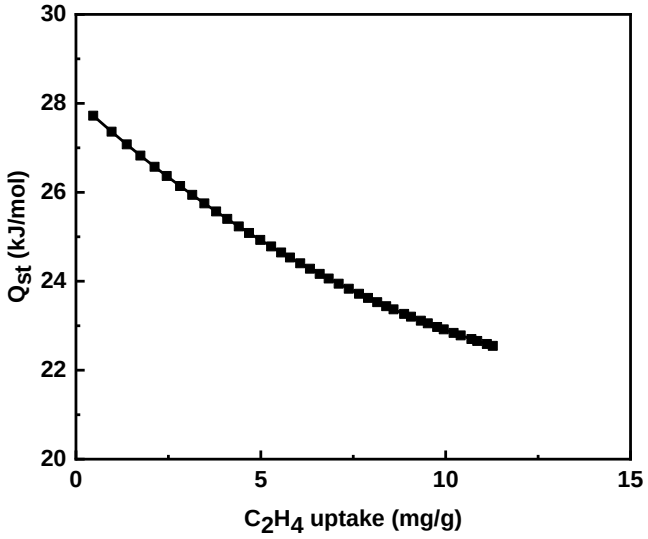

Figure S51. Isosteric Heat of C_2H_4 Adsorption of **C_{10}-AzoCOF**.

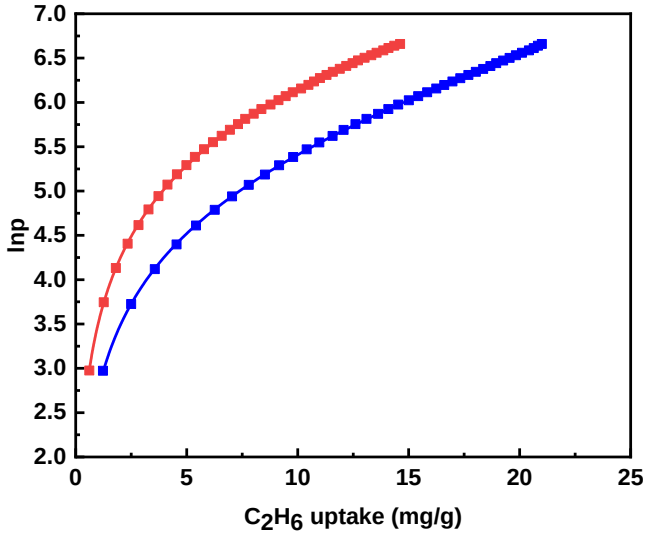

Figure S52. Virial Analysis of C_2H_6 Adsorption Isotherms of **C_{10}-AzoCOF** at 273 K (blue) and 295 K (red).

Table S18. Virial Equation Fitting Results of C_2H_6 Adsorption of **C_{10}-AzoCOF**.

a_0	a_1	a_2	a_3	a_4	a_5	b_0	b_1	b_2	R^2
-2731.76	-29.1441	2.00237	0.17474	-0.00825	0.000147568	12.68565	0.17075	-0.01338	0.99995

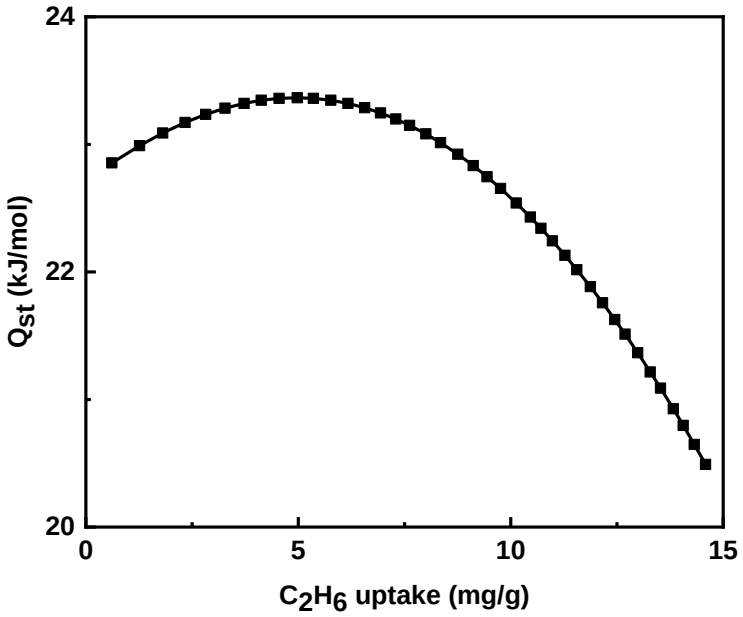

Figure S53. Isosteric Heat of C_2H_6 Adsorption of **C_{10}-AzoCOF**.

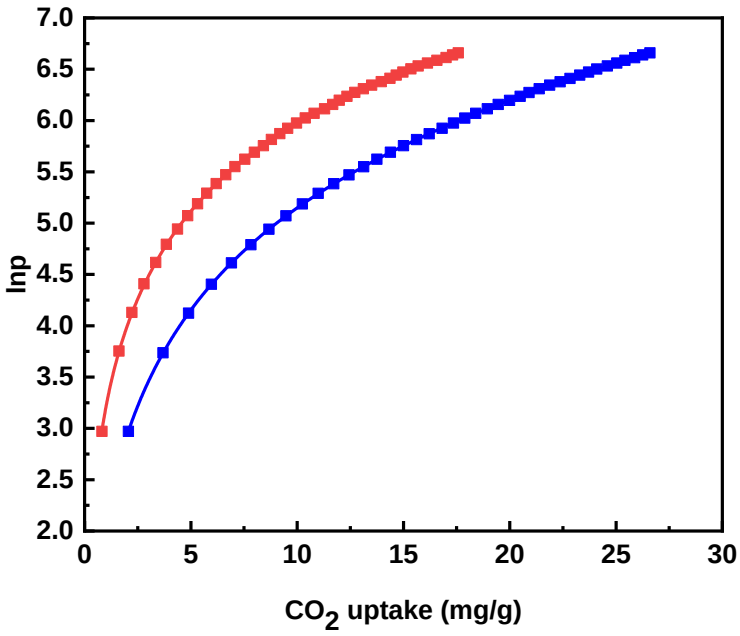

Figure S54. Virial Analysis of CO_2 Adsorption Isotherms of **C_{10}-AzoCOF** at 273 K (blue) and 295 K (red).

Table S19. Virial Equation Fitting Results of CO_2 Adsorption of **C_{10}-AzoCOF**.

a_0	a_1	a_2	a_3	a_4	a_5	b_0	b_1	b_2	R^2
-4159.98	147.5614	-4.88077	0.19312	-0.00531	5.87E-05	17.18331	-0.36841	0.00433	0.99997

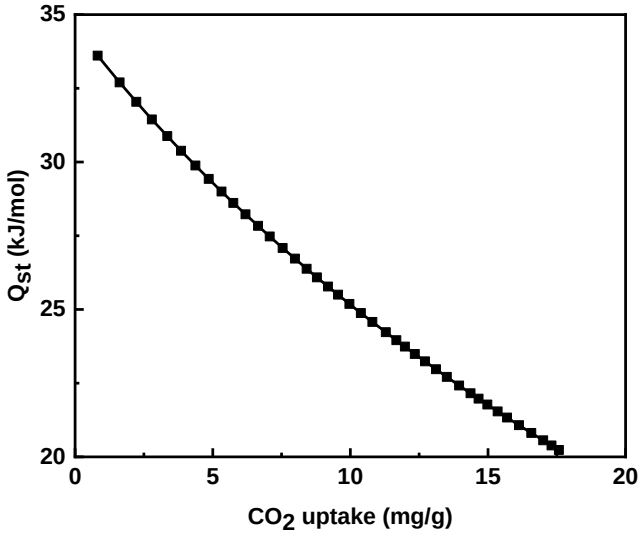

Figure S55. Isosteric Heat of CO_2 Adsorption of **C_{10}-AzoCOF**.

10. Gas adsorption properties of H-COF

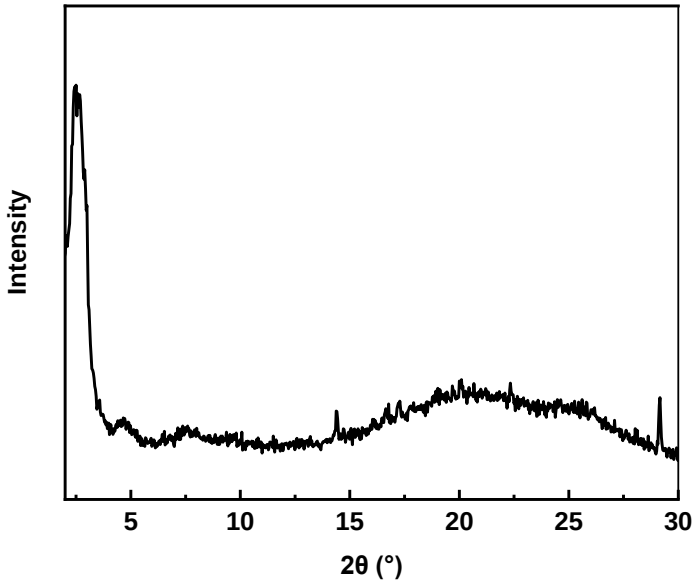

Figure S56. PXRD patterns of **H-COF**.

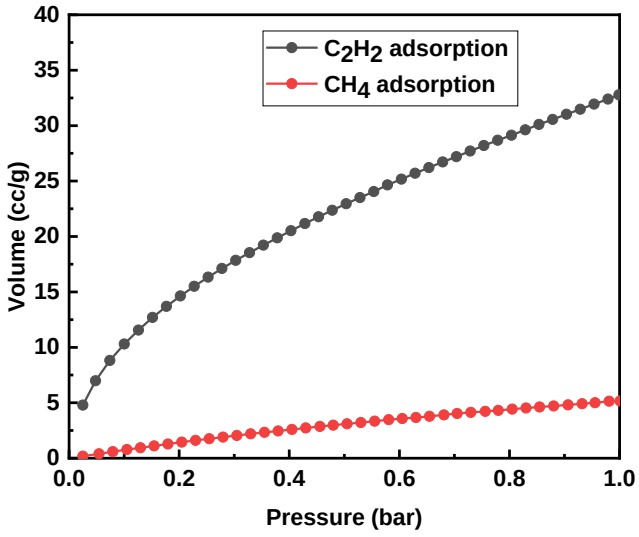

Figure S57. C_2H_2 and CH_4 adsorption isotherms of **H-COF** at 273 K.

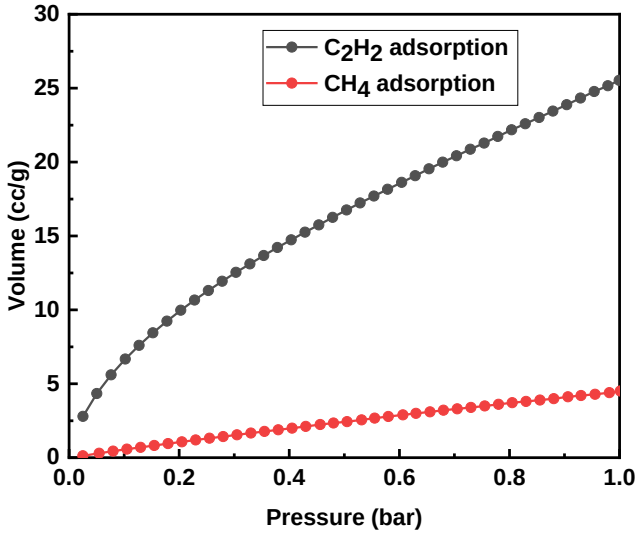

Figure S58. C_2H_2 and CH_4 adsorption isotherms of **H-COF** at 295 K.

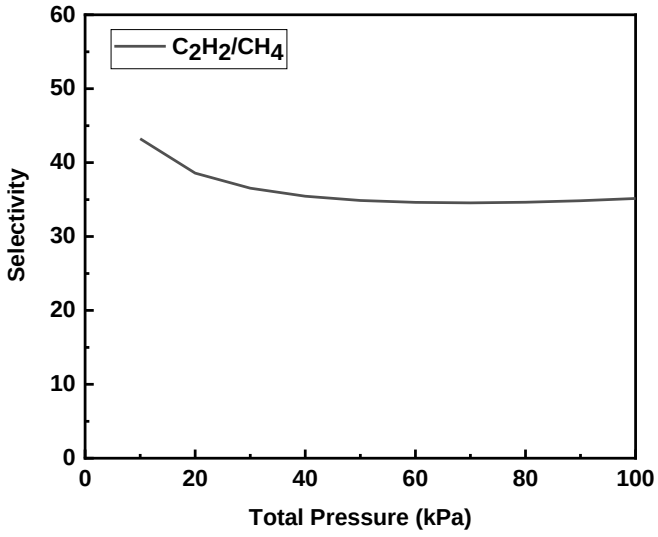

Figure S59. IAST selectivity with 50:50 ratio of C_2H_2/CH_4 gas mixture of **H-COF** at 273 K.

11. Estimation of adsorption heat of H-COF

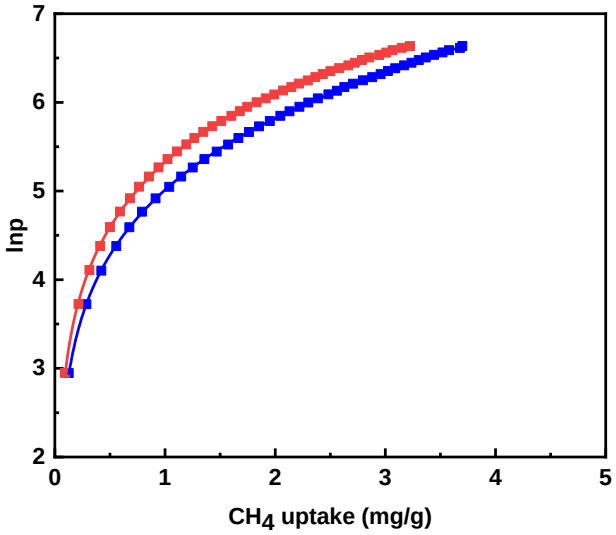

Figure S60. Virial Analysis of CH_4 Adsorption Isotherms of **H-COF** at 273 K (blue) and 295 K (red).

Table S20. Virial Equation Fitting Results of CH_4 Adsorption of **H-COF**.

a_0	a_1	a_2	a_3	a_4	a_5	b_0	b_1	b_2	R^2
-1080.94	-222.048	218.153	-82.9859	21.84914	-2.14645	8.99023	0.49194	-0.26413	0.99993

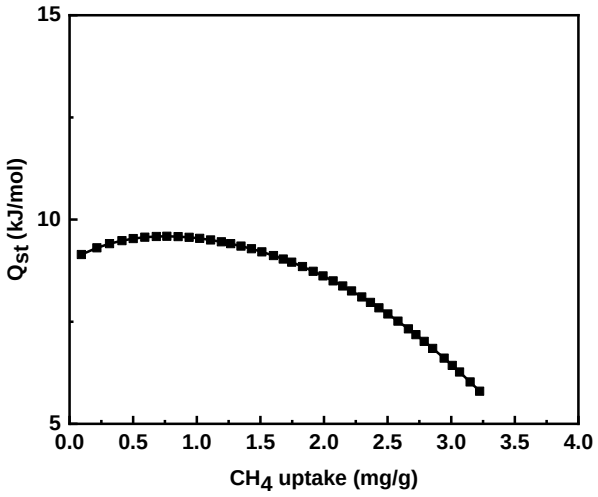

Figure S61. Isosteric Heat of CH_4 Adsorption of **H-COF**.

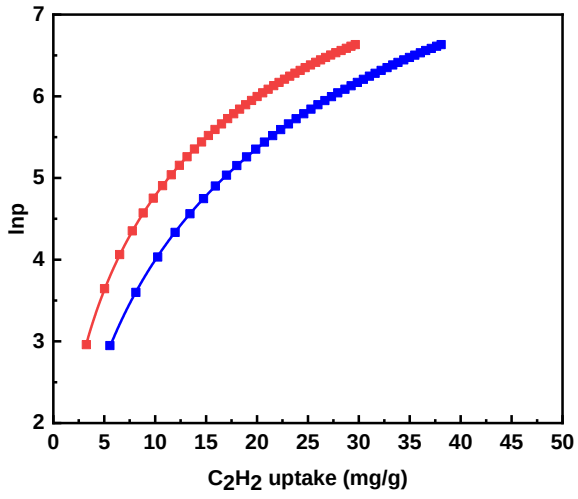

Figure S62. Virial Analysis of C_2H_2 Adsorption Isotherms of **H-COF** at 273 K (blue) and 295 K (red).

Table S21. Virial Equation Fitting Results of C_2H_2 Adsorption of **H-COF**.

a_0	a_1	a_2	a_3	a_4	a_5	b_0	b_1	b_2	R^2
-3549.93	81.83462	-2.45322	0.10993	-0.00223	1.83E-05	13.2881	-0.08144	-0.00204	0.99999

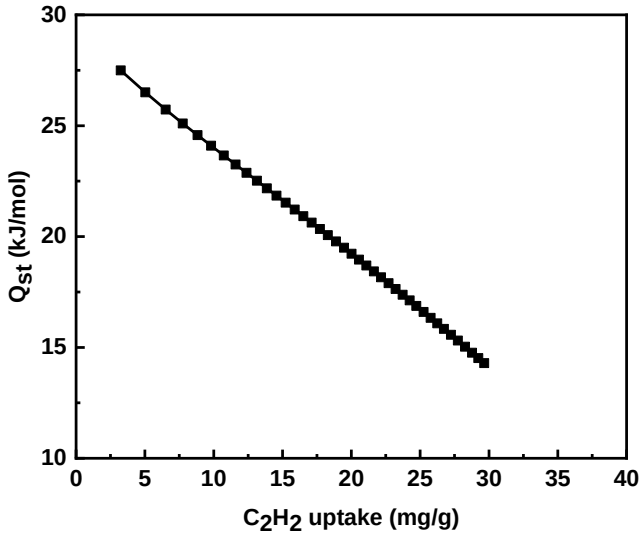

Figure S63. Isosteric Heat of CH_4 Adsorption of **H-COF**.

12. TEM image of AzoCOF

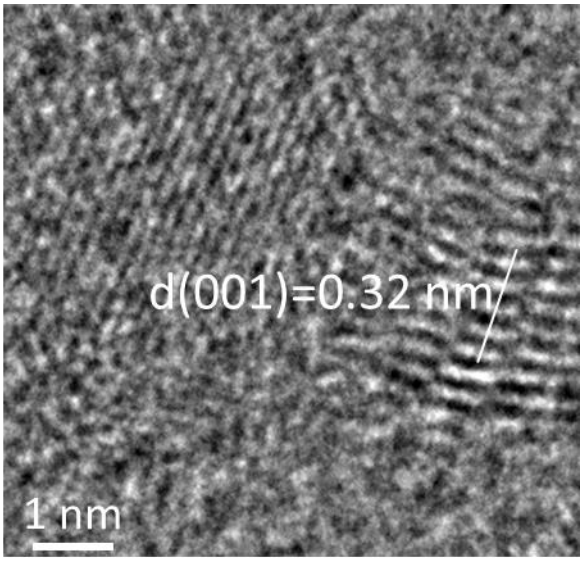

Figure S64. TEM Image of **Tg-AzoCOF**.

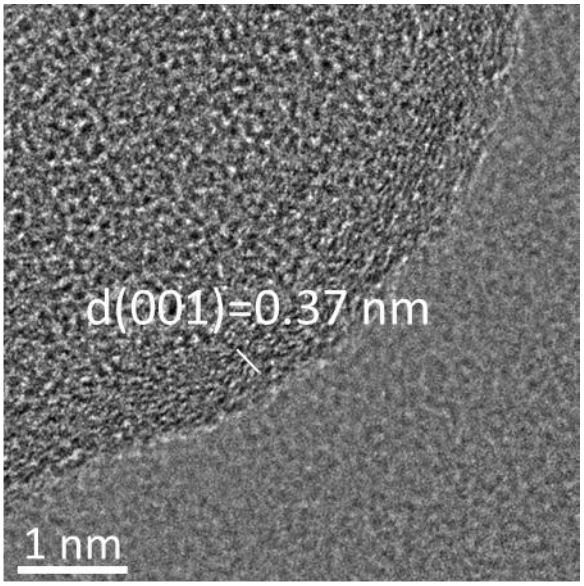

Figure S65. TEM Image of **H-AzoCOF**.

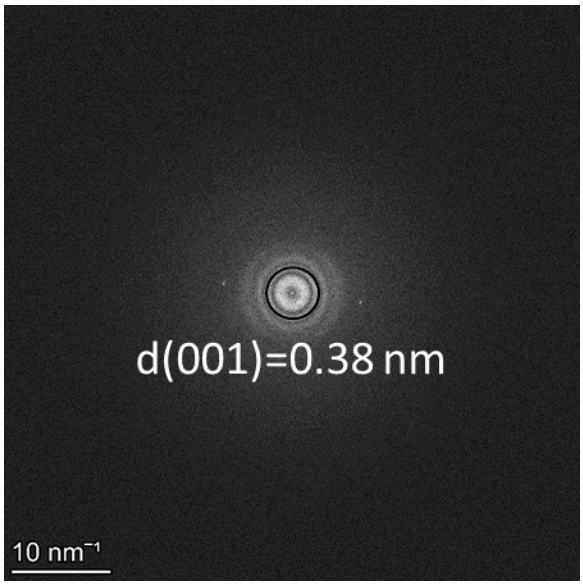

Figure S66. SAED Image of **C_{10}-AzoCOF**.

13. NMR spectra of new compounds

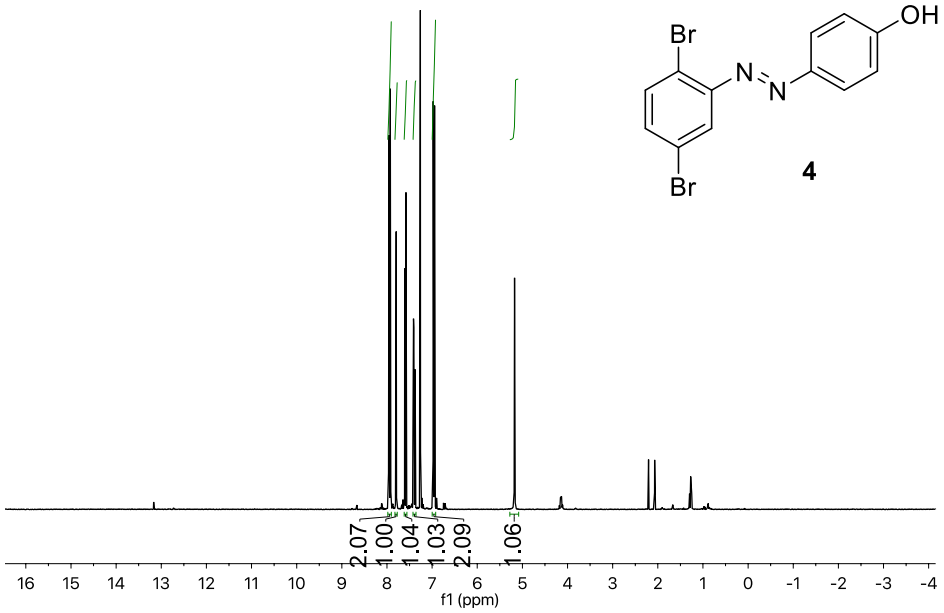

Figure S67. HNMR of Compound **4** in $CDCl_3$

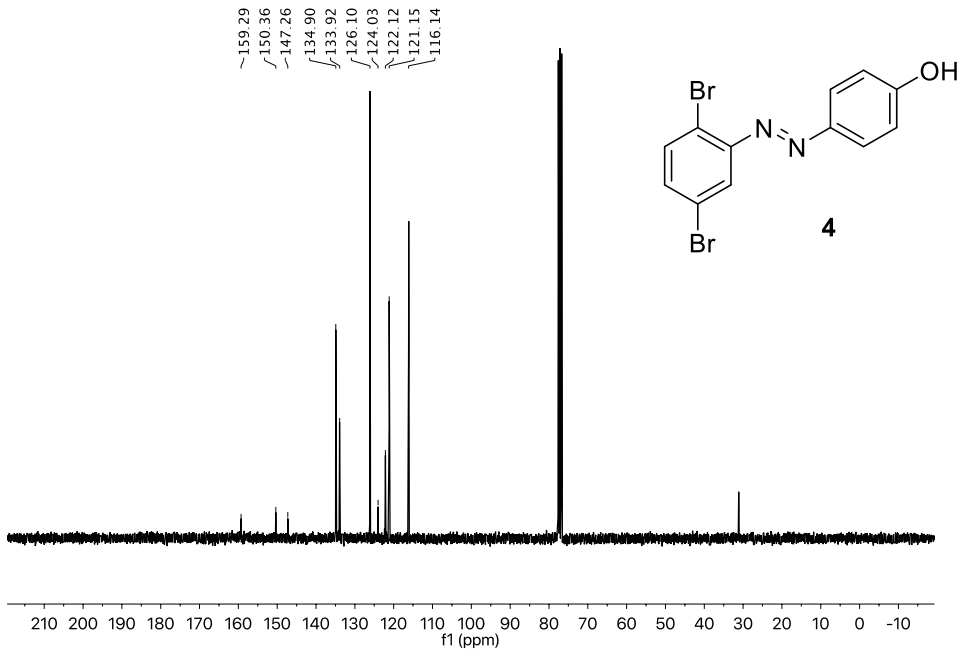

Figure S68. ^{13}CNMR of Compound **4** in $CDCl_3$

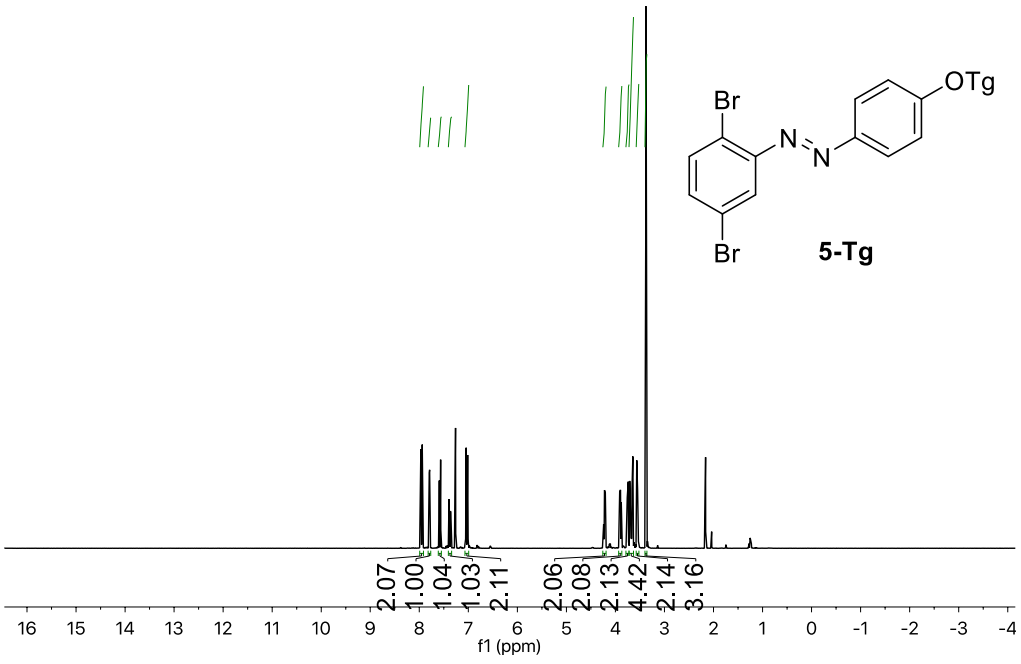

Figure S69. HNMR of Compound **5-Tg** in $CDCl_3$

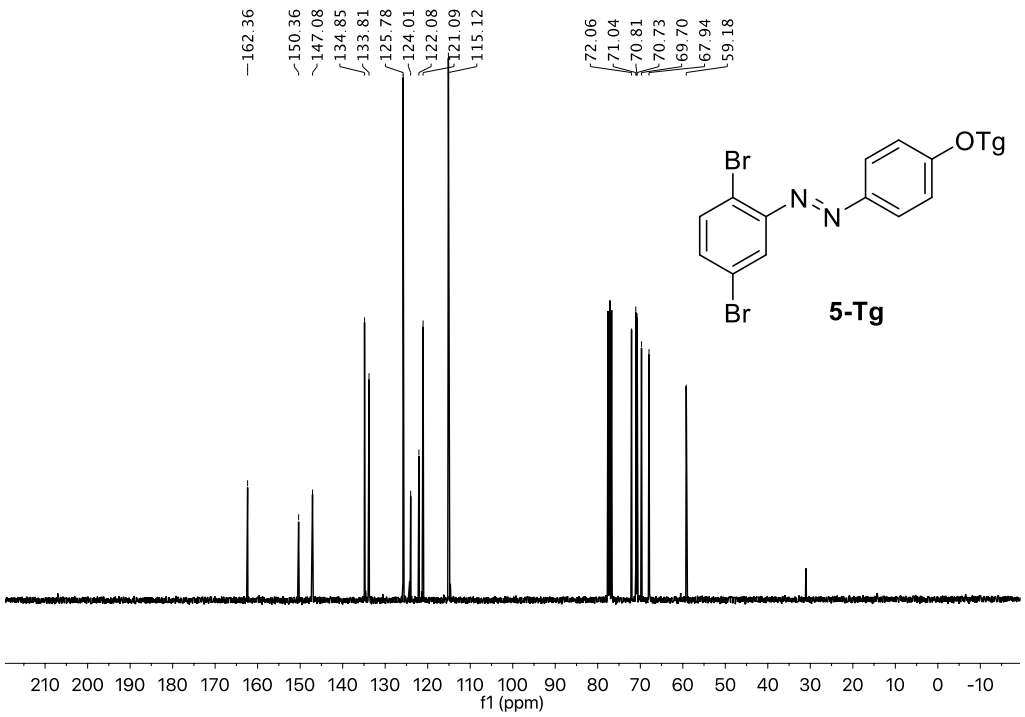

Figure S70. ^{13}CNMR of Compound **5-Tg** in $CDCl_3$

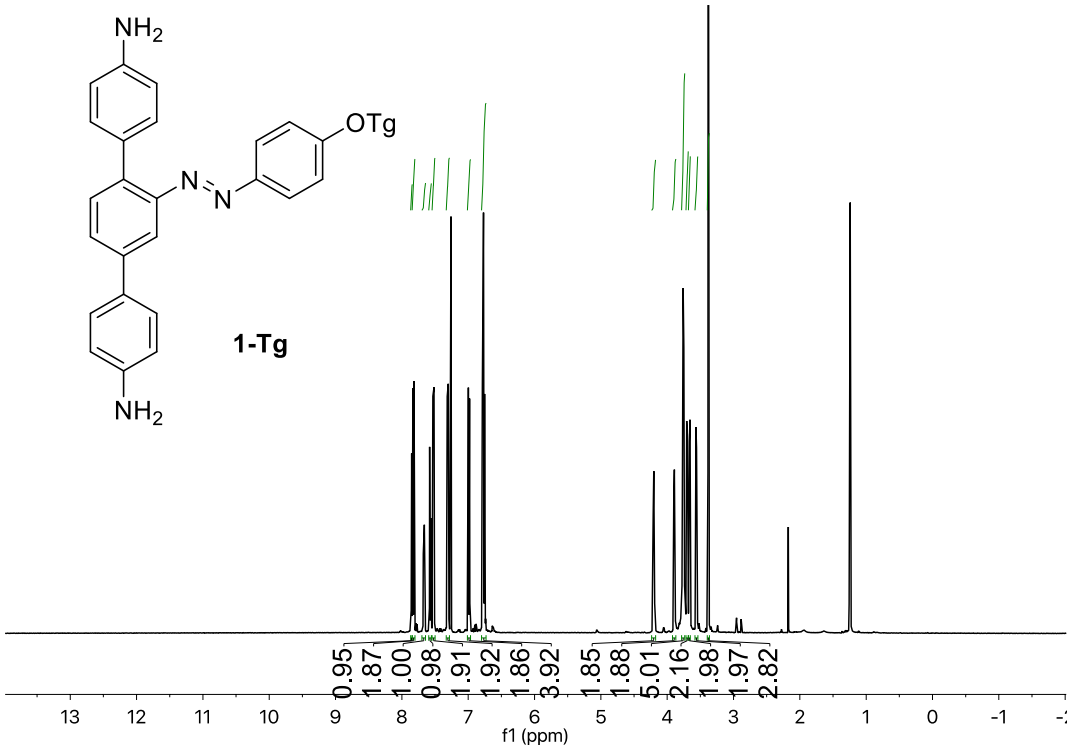

Figure S71. HNMR of Compound **1-Tg** in $CDCl_3$

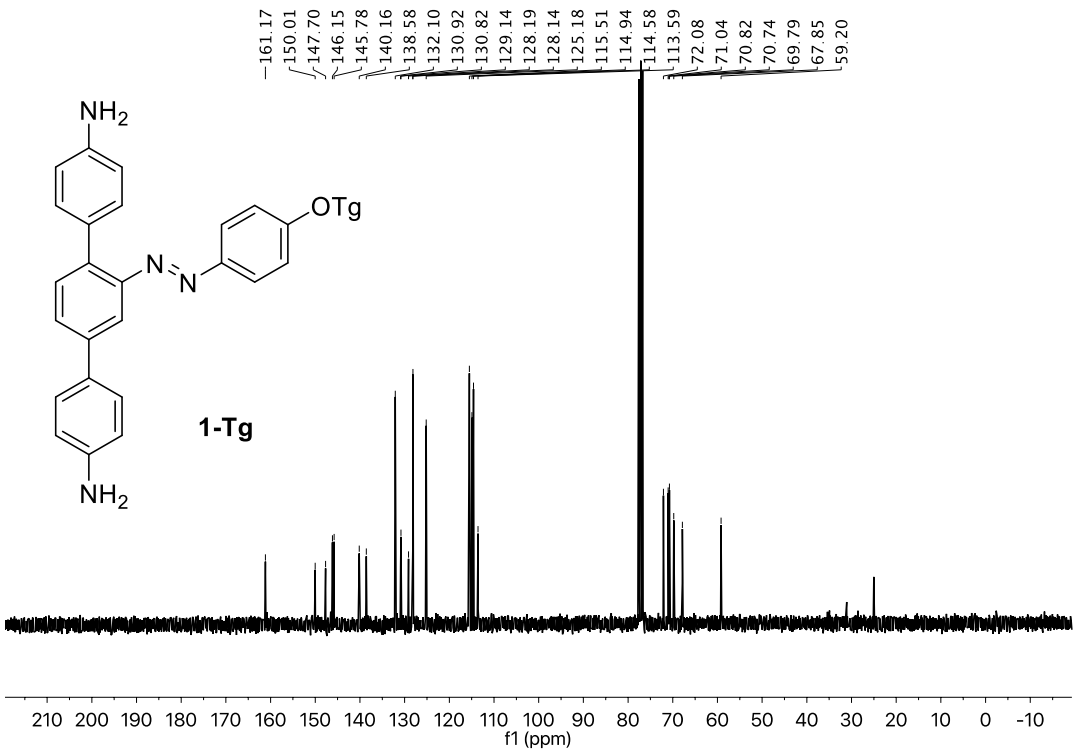

Figure S72. ^{13}CNMR of Compound **1-Tg** in $CDCl_3$

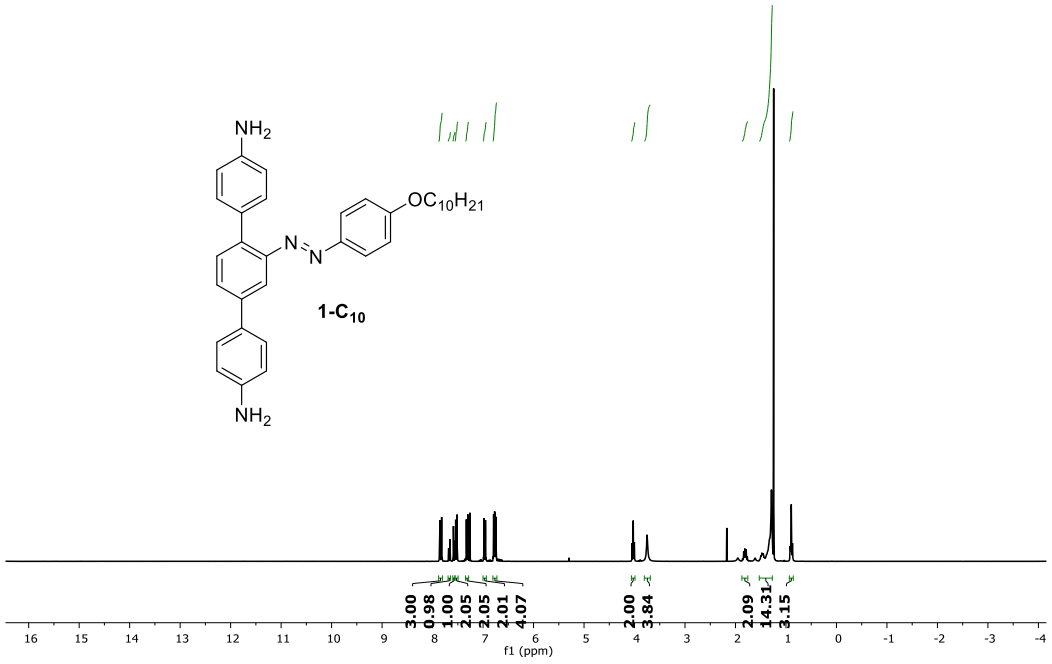

Figure S73. HNMR of Compound **1-C_{10}** in $CDCl_3$

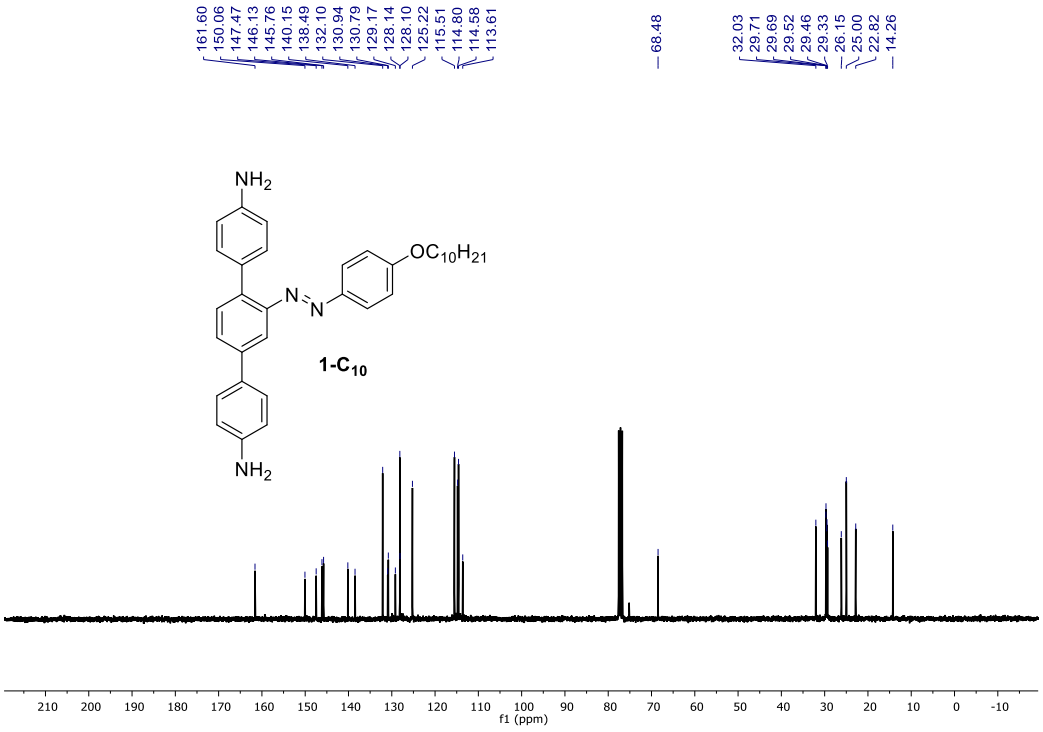

Figure S74. ^{13}CNMR of Compound **1-C$_{10}$** in $CDCl_3$

Reference

1. Zhu, Y.; Zhang, W., Reversible Tuning of Pore Size and CO2 Adsorption in Azobenzene Functionalized Porous Organic Polymers. *Chem. Sci.* **2014,** *5* (12), 4957-4961.
2. Zhang, M.; Li, L.; Lin, Q.; Tang, M.; Wu, Y.; Ke, C., Hierarchical-Coassembly-Enabled 3D-Printing of Homogeneous and Heterogeneous Covalent Organic Frameworks. *J. Am. Chem. Soc.* **2019,** *141* (13), 5154-5158.
3. Wei, T.; Jung, J. H.; Scott, T. F., Dynamic Covalent Assembly of Peptoid-Based Ladder Oligomers by Vernier Templating. *J. Am. Chem. Soc.* **2015,** *137* (51), 16196-16202.